Influence of atmospheric nutrients on primary productivity in a coastal upwelling region

Katherine R. M. Mackey,[1,2] Gert L. van Dijken,[3] Simran Mazloom,[4] Andrea M. Erhardt,[2,4] John Ryan,[5] Kevin R. Arrigo,[3] and Adina Paytan[2]

Received 30 November 2009; revised 21 July 2010; accepted 28 September 2010; published 10 December 2010.

[1] Atmospheric deposition is an important source of nutrients to the coastal and open ocean; however, its role in highly productive upwelling regions like coastal California has not been determined. Approximately 0.1%–0.2% of new production is attributable to atmospheric deposition of nitrogen (N) annually, but if the estimate is expanded to encompass the effects of iron (Fe), aerosols may support 1%–2% of new production on average, and up to 5% on days with high deposition fluxes. Laboratory culture and in situ incubation experiments confirm the bioavailability of N from dry deposition in this region. A significant positive relationship between aerosol optical thickness and chlorophyll *a* derived from the Moderate Resolution Imaging Spectroradiometer is observed for the summer months and is stronger offshore than near the coast. Moreover, the portion of productivity supported by atmospheric deposition is higher on days without upwelling and during El Niño periods when nutrient input from upwelling is suppressed, a phenomenon that could become more prevalent due to climate warming. Expanding the results from California, we estimate that dry deposition could increase productivity in other major coastal upwelling regions by up to 8% and suggest that aerosols could stimulate productivity by providing N, Fe, and other nutrients that are essential for cell growth but relatively deplete in upwelled water.

Citation: Mackey, K. R. M., G. L. van Dijken, S. Mazloom, A. M. Erhardt, J. Ryan, K. R. Arrigo, and A. Paytan (2010), Influence of atmospheric nutrients on primary productivity in a coastal upwelling region, *Global Biogeochem. Cycles*, *24*, GB4027, doi:10.1029/2009GB003737.

1. Introduction

[2] Marine productivity is influenced by numerous processes ranging from phytoplankton community succession to global biogeochemical cycles. Among these processes, those contributing to the supply or regeneration of biologically important nutrients are particularly influential in determining productivity rates. Atmospheric deposition, which includes both precipitation (wet deposition) and dry deposition of aerosols and gases, can stimulate productivity by providing macronutrients as well as trace metals in areas of the ocean where productivity is nutrient limited [*Paerl*, 1985; *Peierls and Paerl*, 1997; *Jaworski et al.*, 1997; *Seitzinger and Sanders*, 1999; *Paerl et al.*, 1999]. By enhancing ocean productivity and carbon sequestration, atmospheric deposition also influences atmospheric carbon dioxide concentrations and climate. Accordingly, understanding the role of atmospheric deposition in influencing ocean productivity within different marine ecosystems is important.

[3] Atmospheric deposition contributes substantially to the nutrient inventories of oligotrophic ocean environments [*Duce et al.*, 2008]. Low-nutrient availability in these regions stems from a scarcity of external nutrient sources, including fluvial and groundwater inputs, such that the relative contribution of atmospheric nutrients is significant. In the Atlantic Ocean, dry deposition both provides nitrogen (N) [*Duce*, 1986; *Prospero et al.*, 1996; *Jaworski et al.*, 1997; *Paerl et al.*, 2002] and stimulates N_2 fixation by providing phosphorus (P) and iron (Fe) to diazotrophs [*Mills et al.*, 2004; *Chen and Siefert*, 2004]. In the North Pacific, it has been suggested that 40%–70% of nitrate is derived from terrestrial aerosol sources [*Prospero and Savoie*, 1989]; however, it should also be noted that wet deposition (rainfall) can, at times, contribute at least as much N and Fe as dry deposition [*Herut et al.*, 1999; *Nadim et al.*, 2001; *Paerl et al.*, 2002]. Atmospheric (mostly aerosol) deposition also supports marine productivity in the oligotrophic Red Sea

[1]Department of Civil and Environmental Engineering, Stanford University, Stanford, California, USA.
[2]Institute of Marine Science, University of California, Santa Cruz, California, USA.
[3]Department of Environmental Earth System Science, Stanford University, Stanford, California, USA.
[4]Department of Geological and Environmental Sciences, Stanford University, Stanford, California, USA.
[5]Monterey Bay Aquarium Research Institute, Moss Landing, California, USA.

0886-6236/10/2009GB003737

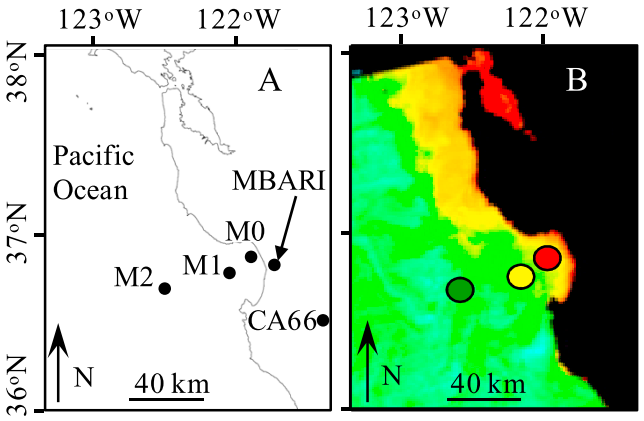

Figure 1. (a) Map showing locations of the long term stations M0, M1, and M2 in Monterey Bay, the location of the aerosol autosampler at the Monterey Bay Aquarium Research Institute (MBARI), and the location of the National Atmospheric Deposition Program precipitation monitoring station (CA66) at Pinnacles National Monument; and (b) example composite image of Chl *a* showing locations of the three "blotch" areas applied to obtain spatially averaged MODIS data using SeaDAS.

and the Mediterranean Sea, where it supplies bioavailable N and P [*Chen et al.*, 2007; *Paytan et al.*, 2009; *Herut et al.*, 1999], is an important source of new (nonregenerated) N to mesotrophic coastal areas [*Paerl and Fogel*, 1994; *Valigura et al.*, 1996; *Jickells*, 1998; *Herut et al.*, 1999], and has been an important source of Fe in high nutrient low chlorophyll (HNLC) regions over geologic time scales [*Martin and Fitzwater*, 1988].

[4] The extent to which atmospheric deposition contributes to production in highly productive coastal upwelling areas, such as the California coast, has not been elucidated. Coastal areas account for only 15% of the ocean surface area but are responsible for half of global marine primary production [*Wollast*, 1991] and support up to 90% of global fish catches [*Pauly et al.*, 2002]. High productivity in upwelling regions results from introduction of deepwater nutrients, principally N, to the euphotic zone where they are taken up by phytoplankton [*Chavez and Messie*, 2009; *Codispoti et al.*, 1982]. However, because they are located along continental margins, many upwelling regions also receive substantial amounts of nutrients via atmospheric deposition. It is therefore important to estimate the contribution of atmospheric deposition to new N in these regions. This contribution could be important during nonupwelling periods when deepwater N inputs are small.

[5] Monterey Bay is an open, deep embayment (>1000 m) on the central coast of California. Euphotic zone depths typically range from 30 to 60m, while mixed layer depths are generally somewhat shallower (10–40 m) [*Olivieri and Chavez*, 2000]. Three long-term oceanographic observational stations are located in Monterey Bay (Figure 1a). Station M0 is closest to shore and is most influenced by coastal and within-bay processes. M1 is situated directly downstream of a major upwelling current, and M2 is the most oceanic of the stations and is less influenced by seasonal upwelling [*Pennington and Chavez*, 2000].

[6] In this study, we assessed the importance of dry and wet deposition in supporting primary productivity in the California upwelling system. We used soluble nutrient measurements from locally collected aerosol particles (PM10) together with an atmospheric deposition model to (1) estimate the flux of new N and other nutrients from dry deposition and (2) identify differences in nutrient content for aerosol particles originating from different geographical sources. Phytoplankton growth experiments are used to demonstrate the bioavailability of N from these aerosol samples. We used oceanographic, atmospheric, and satellite data to (1) characterize the relationship between the timing and extent of dry deposition and chlorophyll abundance and (2) demonstrate spatial and temporal differences in the relationship between dry deposition and phytoplankton growth in coastal and offshore waters.

2. Methods

2.1. Aerosol Particle Collection

[7] Aerosol particle samples were collected using a Dichotomous Partisol-Plus sequential air sampler (Model 2025, Thermo Scientific) located at the Monterey Bay Aquarium Research Institute (Figure 1a) from June 2008 through January 2009. Each sample represents aerosol particles collected continuously over 2 days. The sampler was placed in a remote area at the site, removed from the direct local impact that could potentially contaminate the samples (e.g., proximity to parking lots and roads). The sampler was located about 10 m above ground and 30 m from the shore line and had an airflow rate of 1.67 L min^{-1} for collecting particulate matter 2.5–10 μm in diameter (the "coarse" fraction) and a flow rate of 15.0 L min^{-1} for particulate matter <2.5 μm in diameter (the "fine" fraction). Aerosol particle samples were collected on 47 mm glass fiber filters (Whatman). Prior to sample collection, filters were ashed at 450°C for 5 h, soaked for 2 days in trace metal grade hydrochloric acid (Sigma), soaked (1 day), and thoroughly rinsed with MilliQ water, dried in a laminar flow hood, and stored individually in acid cleaned polystyrene Petri dishes inside new plastic bags. Filters and Petri dishes were weighed together before and after sample collection, and the aerosol particle mass on the filter was calculated as the difference. Samples were stored frozen prior to analysis. Our aerosol concentrations (mg m^{-3} of air) are in good agreement with data collected at terrestrial sites in northern California [*Wells et al.*, 2007; *John et al.*, 1973; *Herner et al.*, 2005], lending support to their credibility and lack of local contamination.

2.2. Aerosol Particle Chemistry

[8] A total of 14 and 11 sampling dates were randomly selected from the summer and winter filter sets, respectively, and the fine and coarse filter samples for each date were extracted separately for a total of 50 extracts. All sample processing was conducted within a laminar flow hood in a clean lab using acid cleaned equipment and storage bottles.

The soluble fraction was extracted from the aerosol particle samples following *Buck et al.* [2006]. An aerosol particle sample (e.g., the 47 mm filter) was placed on an acid washed filter tower, and 100 mL MilliQ water was filtered through the sample allowing 10 s of exposure under gentle vacuum pressure. (This method extracts >99% of soluble ions in the first 100 mL of water based on successive filtrations with the same filter [*Buck et al.*, 2006]). Soluble N concentrations are similar in extractions using MilliQ water and seawater [*Buck et al.*, 2006; *Chen et al.*, 2006].

[9] Five operational filter blanks were analyzed along with the sample filters, and their average filtrate concentrations were subtracted from the sample nutrient concentrations as described below. A 10 mL aliquot of each filtrate sample was analyzed for total oxidized nitrogen (NO_x) and ammonium (NH_4) following *Hansen and Koroleff* [1999] on a flow injection autoanalyzer (FIA, Lachat Instruments Model QuickChem 8000). The FIA was fully automated, and peak areas were calibrated using standards prepared in MilliQ water over a range of 0–60 μmol L^{-1} for NO_x and 0–15 μmol L^{-1} for NH_4. The detection limits based on 3 times the standard deviation of five blank (pure MilliQ water) measurements were 0.42 μmol L^{-1} for NO_x and 0.24 μmol L^{-1} for NH_4.

[10] A 10 mL aliquot of the aerosol filtrate was concentrated 10-fold by evaporation to dryness at 55°C in a trace metal clean Teflon tube and resuspension in 1 mL of 2% trace metal grade nitric acid. These concentrated samples were analyzed for sodium (Na), iron (Fe), and total soluble phosphorus (P) on an inductively coupled plasma mass spectrometer. Peaks were calibrated using standards prepared in 2% nitric acid over a range of 1–10 ppm. The detection limits based on 3 times the standard deviation of eight 2% nitric acid blank measurements were 11.249 μg L^{-1} Na, 0.412 μg L^{-1} Fe, and 0.71 μg L^{-1} P. Our measurements report soluble Fe concentrations in pure water; however, Fe solubility in seawater might be lower than in pure water [*Spokes and Jickells*, 1996; *Buck et al.*, 2006; *Chen et al.*, 2006; *Bonnet and Guieu*, 2004]. Moreover, Fe arriving on the ocean surface is removed rapidly through precipitation and scavenging in addition to biological uptake by phytoplankton and bacteria. Accordingly, our estimates of soluble Fe deposition and uptake therefore represent an upper limit of bioavailable Fe enrichment by aerosol particles to surface waters.

2.3. Air Mass Back Trajectories and Wind Directions

[11] Seven-day air mass back trajectories were generated via a kinematic trajectory analysis using atmospheric data collected at 291 stations worldwide following National Centers for Environmental Prediction (NCEP) analyses (http://croc.gsfc.nasa.gov/aeronet/index.html). Error in the air mass back trajectory (AMBT) simulation increases as the model steps further back in time. The AMBTs are therefore useful as a general guide for air mass provenance, particularly for days immediately preceding the date entered in the model. Sea level AMBTs were determined for the Monterey Bay AERONET (aerosol robotic network) station (36.59255°N, 121.85487°W). Daily in situ wind velocity data were obtained from the live access server for station M2 (http://www.mbari.org/oasis/).

2.4. Estimation of Dry Deposition Nutrient Fluxes

[12] The dry deposition speed of an aerosol particle is the sum of its sedimentation speed (V_s) and its dry deposition against aerodynamic and diffusion resistances at the air-water interface. The sedimentation speed for particles less than 20 μm can be calculated by the following equation [*Jacobson*, 2005],

$$V_s = \frac{2r^2(\rho_p - \rho_a)g}{9\eta} G, \quad (1)$$

where r is the particle radius (cm), ρ_p and ρ_a are the densities of the particle and air, respectively (g cm^{-3}), η is the dynamic viscosity of air (g cm^{-1} s^{-1}), g is the acceleration due to gravity (cm s^{-2}), and G is the Cunningham slip-flow correction factor [*Cunningham*, 1910; *Davies*, 1945; *Jacobson*, 2005]. (G makes the equation valid for both Stokes and slip flow). An average particle density of 2.5 g cm^{-3} was assumed for all aerosol particles [*Lewis and Schwarts*, 2006; *Chen et al.*, 2007], because particles in our samples were likely dominated by mineral dust and sea salt based on composition and air mass back trajectory analysis.

[13] For the coarse aerosol fraction comprising particulate aerosols between 2.5 and 10 μm, the effect of gravity supersedes the effect of resistance at the boundary layer, and dry deposition is dominated by the sedimentation speed V_s. As the exact grain size distribution for each aerosol sample was unknown, we assumed a dry deposition speed of 0.8 cm s^{-1} for the coarse fraction based on equation (1) for particles 10 μm in diameter. This speed is similar to values found for other regions [*Chen et al.*, 2007, 2008]. The dry deposition speed for particles 2.5 μm in diameter was approximately 0.05 cm s^{-1}; therefore, the maximum possible error associated with our estimate would be 16-fold if all of the particles in the coarse fraction were 2.5 μm in diameter (unlikely). Sea spray also contributes to coastal aerosols. The maximum possible error associated with our density assumption of 2.5 g cm^{-3} would overestimate dry deposition speed by 2-fold to 3-fold if all aerosol particles were sea spray, which has the same density as seawater (1.03 g cm^{-3}). Under the same atmospheric conditions assumed in our calculations, a model by *Slinn and Slinn* [1980] predicts a dry deposition speed of 3.0 cm s^{-1}, and *Williams* [1982] predicts a speed of ~1.0 cm s^{-1} for particles 10 μm in diameter. Therefore, while 0.8 cm s^{-1} is a high-end estimate based on particle size using equation (1), it is conservative compared to other values that have been assumed for dry deposition speed of particles on natural waters [e.g., *Duce et al.*, 1991; *Buck et al.*, 2006].

[14] For particles below 1 μm, dry deposition is dominated by diffusion rather than gravitational forces and is calculated based on the particle's aerodynamic resistance (determined by the friction wind speed, height above the sea surface, the surface roughness length of the particle, and a potential temperature gradient) and the resistance to molecular diffusion in the laminar sublayer (determined by the surface roughness length for momentum, kinematic viscosity, mass diffusivity, thermal diffusivity, and friction wind speed.) *Chen et al.* [2007] showed that very similar

Table 1. Water Soluble Nutrient and Metal Concentrations and Depositional Fluxes for Summer and Winter Aerosol Samples

	Concentration (μg m^{-3})				Flux (μg m^{-2} d^{-1})			
	Minimum	Maximum	Mean	SE	Minimum	Maximum	Mean	SE
				Summer				
TSP	31	160	69	3.5	12	89	34	2.0
Na	2.5	19	9.1	1.2	108	9737	4771	668
Fe	0.0017	0.011	0.0051	0.00074	0.096	5	1.5	0.37
NOx	0.14	1.2	0.37	0.073	33	233	87	14
NH4	0.11	0.53	0.25	0.032	16	92	36	5.2
P	0.0018	0.0061	0.0039	0.00037	0.095	2.3	1.5	0.18
				Winter				
TSP	15	102	50	5.4	7.4	54	24	2.9
Na	1.2	11	5.2	0.92	320	6160	2777	546
Fe	0.0043	0.015	0.0075	0.001	0.7	5.4	2.2	0.41
NOx	0.22	1.2	0.67	0.095	58	152	103	8.5
NH4	0.22	1.3	0.57	0.11	36	79	57	3.6
P	0.0035	0.0092	0.0062	0.00054	1.0	4.1	2.2	0.27

velocities (within 10%) were predicted for small particles of different sizes (e.g., particles <2.5 μm within the fine fraction) using the model by *Jacobson* [2005]. Accordingly, we assumed a dry deposition speed of 0.05 cm s^{-1} for the fine fraction based on equation (1) for particles 2.5 μm in diameter. The dry deposition speed decreases with particle diameter, reaching a minimum for particles ~1 μm in diameter. Dry deposition speeds increase with decreasing particle diameter for particles <1 μm because diffusion resistances dominate deposition speeds rather than gravity. The dry deposition speed for particles 1 μm in diameter is 0.01 cm s^{-1}; therefore, the maximum possible error associated with our estimate would be 5-fold if all of the particles in the fine fraction were 1 μm in diameter (unlikely). Similar to the coarse fraction, our estimate is conservative compared to estimates from *Slinn and Slinn* [1980] and *Williams* [1982], which predict speeds of approximately 0.2 cm s^{-1} under the same conditions for particles ~2.5 μm in diameter.

[15] The flux for each nutrient was calculated as the product of the dry deposition speed and the direct determination of the water soluble concentration of the nutrient in each aerosol sample (Table 1). By separating calculations for nutrient fluxes from the coarse and fine fraction measurements, errors stemming from uneven distribution of nutrients between these fractions were minimized. For example, NH_4 and some trace metals generally occur in higher concentrations in fine fractions from anthropogenic high-temperature combustion emissions [*Church et al.*, 1991; *Huebert*, 1980; *Spokes et al.*, 2001], while nutrient species like NO_3, PO_4, and other metals are generally associated with the coarse aerosol fraction [*Savoie and Prospero*, 1982; *Spokes et al.*, 2001; *Duce et al.*, 1991; *Prospero et al.*, 1996].

[16] Our flux estimates are for water soluble nutrients in particulate aerosols but may also include input from gaseous nitrate (as HNO_3), which can contribute substantially to the total N input from dry deposition [*Kouvarakis et al.*, 2001]. Efficient scavenging of HNO_3 occurs when cellulose or glass fiber filters are used [*Appel et al.*, 1980; *Savoie and Prospero*, 1982; *Prospero and Savoie*, 1989; *Schaap et al.*, 2004] and can be as high as 100% when aerosol sea salt content is high [*Appel et al.*, 1980; *Appel et al.*, 1981]. HNO_3 contributes <10%–30% to total NO_3 in the marine boundary layer [*Savoie and Prospero*, 1982; *Huebert*, 1980]. Accordingly, soluble NO_x measurements in our samples could represent up to 30% input from HNO_3, particularly in samples with higher proportions of sea salt.

[17] In contrast to adsorption of NO_3, volatilization of ammonium nitrate from the filter can underestimate soluble nitrate measurements, particularly in samples with low aerosol masses [*Wang and John*, 1988] and under ambient temperatures greater than 25°C [*Schaap et al.*, 2004]. While we cannot quantify the error from volatilization, we expect it to be small compared to the N concentrations in particulate aerosols given the moderate temperatures at the California coast throughout the year. Further, the relatively high particle load recorded for the majority of coarse fraction samples would minimize volatilization in these sample sets (e.g., <10% error) [*Wang and John*, 1988]. Volatilization may play a larger role (up to 85%–95% loss) in the fine aerosol fraction due to lower overall particle loading; accordingly, our estimates should be taken as a lower limit for the dry deposition of new N to coastal California, particularly for the fine aerosol fraction.

2.5. In situ Data

[18] In situ surface chlorophyll *a* (Chl *a*) measurements were obtained from the three long-term monitoring stations in Monterey Bay (M0, M1, and M2), where they were taken approximately every 3 weeks, and were measured fluorometrically as described elsewhere [*Pennington and Chavez*, 2000] (data courtesy of R. Michisaki and F. Chavez). Daily upwelling index data were obtained from the National Oceanic and Atmospheric Administration (NOAA) Southwest Fisheries Science Center live access server for the Pacific coast at 36°N 120°W (http://las.pfeg.noaa.gov/las6_5/servlets/dataset).

[19] Wet deposition data were obtained from the National Atmospheric Deposition Program database for station CA66, located at Pinnacles National Monument in San Benito County, California (36.4834°N, 121.157°W, elevation 317 m; Figure 1a). Monthly precipitation measurements and annual inorganic N (NH_4 + NO_3) deposition values

were obtained for 2002–2009. N depositions were computed by multiplying the precipitation-weighted mean N concentration (mg/L) for samples meeting the QAQC and data completeness criteria by the total precipitation in centimeters for the summary period. QAQC and data completeness criteria are described on the program's Web site (http://nadp.sws.uiuc.edu). The monitoring station is located ~60 km inland from the coast, and the amount of precipitation recorded at the site could therefore differ from that of Monterey Bay proper. On the basis of annual average precipitation rates provided by the U.S. Geological Survey (http://www.nationalatlas.gov/printable/images/pdf/precip/pageprecip_ca3.pdf), the southern coast of Monterey Bay receives a similar amount of precipitation to station CA66 (ca. 25–50 cm/yr). However, the northern coast of the bay receives slightly higher rainfall (~50–75 cm/yr). The amount for the entire area of Monterey Bay is likely to fall within the range of these values. We note that the chemical composition of precipitation (e.g., NH_4 + NO_3) would not be expected to vary considerably over this distance, and would contribute minimal error to our estimates.

2.6. El Niño Southern Oscillation Indices

[20] Two monthly indices of the El Niño Southern Oscillation (ENSO) were used. The Multivariate ENSO Index (MEI) is calculated from sea level pressure, zonal and meridional components of the surface wind, sea surface temperature, surface air temperature, and total cloudiness fraction of the sky. MEI data were obtained from the NOAA Earth System Research Laboratory (http://www.cdc.noaa.gov/people/klaus.wolter/MEI/). The Southern Oscillation Index (SOI) is based on air pressure differences between Tahiti and Darwin islands, and SOI data were obtained from the Australian Government Bureau of Meteorology (http://www.bom.gov.au/climate/current/). The time series includes data from 2002 to 2009 to overlap with the Moderate Resolution Imaging Spectroradiometer (MODIS) record used in our analyses (2002–2008) and to encompass the period during which our particulate aerosol samples were collected (2008–2009).

2.7. MODIS Satellite Data

[21] Aerosol optical thickness (AOT, 869 nm) and Chl *a* (OC3 algorithm) were determined from satellite images taken by the Moderate Resolution Imaging Spectroradiometer (MODIS) satellite for July 2002 to June 2008 at a resolution of 1 km. The MODIS viewing swath width is 2330 km and scans the entire surface of the Earth every 1–2 days. A total of 2208 level 2 data files (each containing AOT and Chl *a* data) were processed to level 3 using SeaWiFS Data Analysis System (SeaDAS) software by applying identical processing scripts to all files as follows. Each data file was projected, generating new individual image files for AOT and Chl *a*. This step yielded a total of 4416 files. Projected files were binned into 8 day groups, images of low quality (e.g., periods with extensive cloud cover) were removed, and each bin was averaged to create a composite image that represented one 8 day "week." This step yielded a total of 552 images, i.e., 276 separate "weekly" images for each of the parameters.

[22] Aerosol optical thickness and Chl *a* were quantified identically in all composite images. Three areas were designated using the blotch analysis function in SeaDAS. Each blotch was a circular region (~140 km^2) centered on each of the three long-term in situ Monterey Bay monitoring sites M0, M1, and M2 (Figure 1b). The histogram function was applied to each blotch and the mean value for each composite image was recorded. This process was manually repeated for all of the AOT and Chl *a* images. To test if there was a correlation between the timing and magnitude of aerosol optical thickness and Chl *a*, regression analysis of MODIS data was performed. Annual time series, paired correlations, and time-lagged correlations of the composite data were made for each season. "Summer" and "winter" were defined based on annual mean wind stress data from 2002 to 2008 collected at an offshore mooring in Monterey Bay, which shows the winds are from the northwest March through November (weeks 12–37), with intermittent southerly winds November through early March (weeks 1–11 and 38–48).

[23] A potential caveat in computing satellite-derived Chl *a* data is that thick aerosol layers can cause overestimation of Chl *a* by the satellite algorithms due to enhanced backscatter of the wavelengths used to measure Chl *a*. A study by *Volpe et al.* [2009] explored this issue in the Mediterranean Sea, showing that significant correlations between aerosol optical thickness and satellite-derived Chl *a* levels were not always supported by in situ Chl *a* measurements. It was therefore necessary to compare the 8 day averaged Chl *a* levels from MODIS with in situ surface measurements of Chl *a* from the long-term monitoring program in Monterey Bay that were collected at roughly 3 week intervals. The agreement between the in situ and satellite data was acceptable with R^2 values of 0.52, 0.38, and 0.49 for stations M0, M1, and M2, respectively ($p < 0.05$ for all stations). However, regression statistics indicated that MODIS tended to overestimate Chl *a* slightly, particularly at locations closer to shore. The regression slope (m) approached 1 (i.e., when MODIS perfectly predicts in situ Chl *a* levels) with increasing distance from shore, but overestimates Chl *a* ($m < 1$) closer to shore ($m = 0.58$, 0.84, and 0.97 for stations M0, M1, and M2, respectively).

[24] This discrepancy in predictive power likely stemmed from the MODIS atmospheric correction algorithm, which can yield artificially high Chl *a* values in turbid waters and waters containing high levels of colored dissolved organic matter (CDOM), both of which are more prevalent closer to shore. Another possible reason for the discrepancy included the larger spatial and temporal range of values included in the satellite estimates (due to blotch size and image averaging, respectively), whereas in situ measurements were collected at discrete locations and times. Moreover, in situ measurements provide surface water Chl *a* levels only, whereas MODIS integrates deeper within the water column (down to 1 optical depth).

2.8. Phytoplankton Growth Experiments

[25] To determine the bioavailability of N from dry deposition to phytoplankton endemic to coastal California, culture experiments were conducted with three cultured

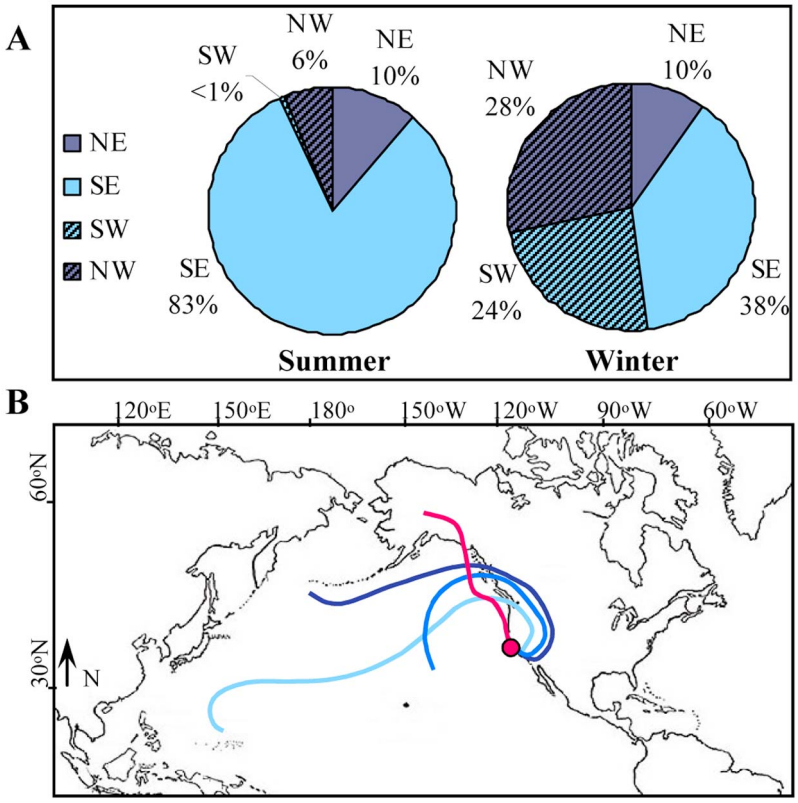

Figure 2. (a) Direction of air mass trajectories arriving at Monterey Bay in the summer and winter based on daily wind velocity measured at station M2. Hatched areas indicate winds blowing to the west, open areas indicate winds blowing to the east, light blue areas indicate winds blowing to the south, and dark blue areas indicate winds blowing to the north. In summer the majority of air masses blow in a southeastern direction parallel to the California coast, while westward winds coming from land are more common in the winter. (b) Example 7 day air mass back trajectories (AMBTs) for Monterey Bay during the summer (red) and winter (blue). AMBTs were generally much more variable in the winter than the summer.

strains of phytoplankton isolated from the southern coast of California and with natural populations of phytoplankton in Monterey Bay. For the culture work, *Synechococcus nigra* CCMP 1284 (collection site: Scripps Institute of Oceanography, 32.8504N 117.2525W) and *Thalassiosira weissflogii* CCMP 1050 (collection site: Del Mar Slough, California, 32.9660N 117.2510W) were obtained from the Provasoli-Guillard National Center for Culture of Marine Phytoplankton (CCMP). *Synechococcus* strain CCMP 2515 (collection site: CalCOFI cruise 93204, 31.9001N 124.1668W) was provided by K. Pennebaker and J. Zehr. Cultures were maintained in F/2 media. Prior to the experiment, cultures were diluted tenfold into media without added N (F/2-NO_3) until stationary growth phase was reached (several days). This step was included to draw down residual N in the inoculum. Cultures were then transferred into fresh media amended with either a full compliment of F/2, including NO_3, or F/2-NO_3 plus natural particulate aerosol extract from samples collected at Monterey Bay. The final NO_x concentration was ~50 mg L^{-1} in aerosol treatment and ~55 mg L^{-1} in F/2 with NO_3 treatment. The amount of aerosol added was calculated to yield aerosol-NO_x similar to the amount of NO_3 in the F/2 media. Treatments were conducted in triplicate. The optical density of the cultures at 750 nm (OD750) was used to evaluate daily cell growth during the 6 day incubation period.

[26] An incubation experiment was also conducted with natural assemblages of phytoplankton from Monterey Bay beginning 4 October 2009 aboard the Research Vessel John Martin. Surface water (1 m depth) was collected from northeast Monterey Bay (36′48.168°N, 121′48.268°W) at midday near the edge of the "red tide incubator" region [*Ryan et al.*, 2008], where moderately high standing stocks of dinoflagellates generally persist. The following treatments were immediately made: "control" which had no addition, "nitrate" which had 25 μM $NaNO_3$ added, and "aerosol" which had 1 mg L^{-1} particulate aerosol added. Treatments were conducted in triplicate in acid washed polycarbonate bottles that were thoroughly rinsed with surface sample water before use. Bottles were kept in an on-deck incubator through which surface water from the Bay was continually pumped to maintain ambient temperature

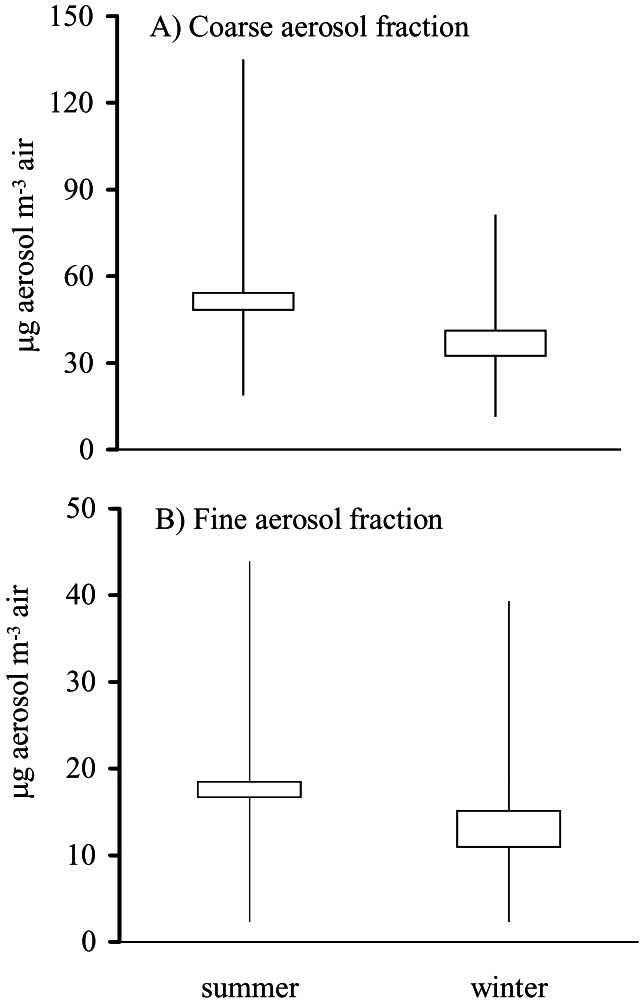

Figure 3. Aerosol concentration for fine and coarse aerosol fractions in summer and winter. Upper and lower box edges depict mean ± SE. Lines show range.

within the Bay. A neutral density shade was used to attenuate sunlight by 50%. After 30 h, Chl *a* was measured according to *Mackey et al.* [2009] with the following modifications: 100 mL aliquots were removed from each bottle and filtered under gentle pressure onto GF/F filters (Whatman). Filters were frozen at −80°C. Chlorophyll extractions were performed for 24 h at 4°C in the dark using 90% acetone, and fluorescence was measured on a Turner fluorometer (Turner Designs 10-AU-005-CE) before and after acidification with 3.7% HCl. Fluorescence was converted to Chl *a* concentration according to *Knap et al.* [1996].

[27] Particulate aerosols used in the incubation were collected as described above and included both fine and coarse fractions. As with the culture experiments, we emphasize that the goal of the experiments was only to determine if the N in dry deposition was bioavailable to phytoplankton in this region. We therefore used relatively large particulate aerosol and NO_3 additions, such that we would be able to see a measurable increase in Chl *a* during the experiment. The NO_3 concentration was selected based on typical NO_3 levels following upwelling in the Bay, and the amount of particulate aerosol added was chosen to roughly double the background concentration of NO_x in the seawater from ~0.5 to ~1 μmol L^{-1}. While this amount of aerosol is higher than would be expected for typical dry deposition events in coastal California, we emphasize that the goal of the experiment was to determine the bioavailability of N in dry deposition, not to test the effects particulate aerosols using typical deposition rates.

3. Results

3.1. Air Mass Sources, Particulate Aerosol Loads, and Nutrient Fluxes

[28] Air mass provenance was determined for summer and winter based on a representative year of wind velocity data collected at station M2 in 2005. Air mass back trajectory (AMBT) analysis of sea level air masses indicated that, during the summer, the majority of air masses originated over the North Pacific Ocean and traveled in a southeastern direction parallel to the California coast before arriving at Monterey Bay, consistent with wind speed data recorded at station M2 (Figure 2a). Winter AMBTs had diverse origins, reflecting the heterogeneous wind patterns recorded at M2 during winter months (Figure 2a). Notably, in the winter about half of the air masses arrived from land (i.e., headed from east to west), while in the summer the vast majority (~93%) arrived from the ocean (i.e., headed from west to east) (Figure 2a). Figure 2b shows several examples of 7 day AMBTs that occurred during our particulate aerosol collection period.

[29] Particulate aerosol composition showed marked differences between seasons and different size fractions. Total suspended particle (TSP) concentrations (μg m^{-3}) determined from all samples collected during the sampling period (i.e., not limited to the 50 extracted filters) were slightly higher in the summer than winter (Table 1 and Figure 3) and higher for the coarse aerosol fraction than the fine fraction (Figure 3). NO_x, NH_4, and soluble P concentrations were higher in the winter than in the summer ($p < 0.05$), although summer particulate aerosols had higher amounts of Na than in winter ($p < 0.05$; Table 1). The ratios of NO_x to P were higher in fine aerosol fractions than in coarse fractions (Figure 4). Mean NO_x/P values were similar for winter and summer in the coarse fraction (~140), whereas fine fraction mean values were higher in winter (~500) than summer (~320). The majority of N deposition was attributed to NO_x, although NH_4 also contributed substantial N. The coarse fraction contributed more N deposition than the fine fraction, and N deposition was slightly higher in winter than summer (Table 2).

3.2. Time Series Data

[30] As expected over this relatively small area, the AOT levels were similar for all three monitoring sites at all times of the year (Figure 5). Aerosol layers generally were thickest in March through June (Figure 5), in agreement with in situ measurements that showed higher particulate aerosol concentrations in the summer (Figure 3). MODIS-derived Chl *a*

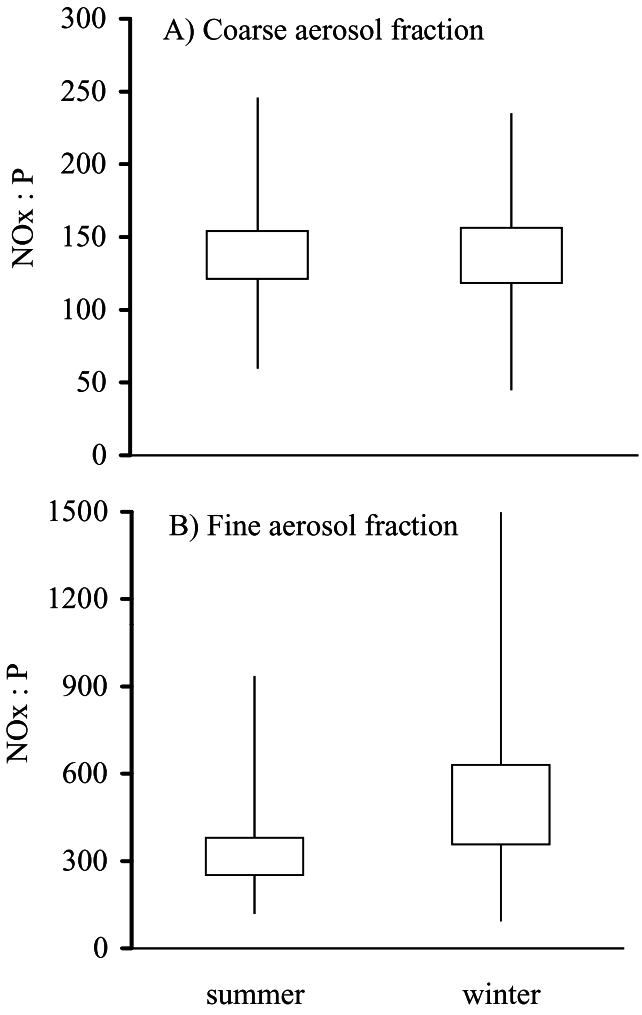

Figure 4. NO_x:P ratios for fine and coarse aerosol fractions in summer and winter. Upper and lower box edges depict mean ± SE. Lines show range.

concentration for the same time interval for the three stations are also shown in Figure 5, and Figure 6 shows annual averages of the AOT and Chl *a* data for the three stations. Chl *a* levels were higher closer to shore and were higher in summer than winter for all sites.

[31] Zonal and meridional components of wind speed (Figures 5d and 5e) were consistent with AMBT model outputs (Figure 2) and indicated that the wind trajectory was predominantly in the southeast direction during summer months. No consistent trajectory was observed for winter.

[32] Rainfall followed a predictable seasonal pattern, generally commencing in October through November and ending in May. Maximum monthly precipitation (Figure 5f) reached up to ~15–20 cm/mo during the wettest winter months (generally December through February), whereas precipitation was negligible during the summer. N input from wet deposition at the closest NADP station averaged 74, 112, 68, 90, 80, 47, and 90 μg N m^{-2} d^{-1} for 2002, 2003, 2004, 2005, 2006, 2007, and 2008, respectively, or 80 ± 8 μg N m^{-2} d^{-1} on average based on annually averaged precipitation levels and N contents.

[33] Long-term monthly averages of daily upwelling indices show that upwelling occurred mostly throughout the spring and summer and was greatest during May through July (Figure 7). Upwelling relaxes and occasionally reverses (i.e., downwelling occurs) during the winter months.

3.3. Correlations Between AOT and Chl *a*

[34] Seasonal differences in the relationship between AOT and Chl *a* might be expected due to different air mass provenances and variable input from other nutrient sources (e.g., upwelling, runoff) in different seasons. No significant relationships were identified for winter at any of the stations based on regression analysis of MODIS data. A statistically significant relationship was identified for stations M1 (p = 0.028, n = 125) and M2 (p = 0.004, n = 122) during the summer and indicated that 3.9%–6.6% of the variability in Chl *a* at these stations correlated with AOT (Table 3). Overall annual regression with the seasonal signal removed by subtracting out the average values of AOT and Chl *a* for each week of the year also indicated that a significant relationship exists between AOT and Chl *a* (for example, at station M2 2.3% of the variability in Chl *a* was attributed to AOT over an annual cycle, p = 0.02, n = 219). Correlations were not improved for regressions with 1 week time-lagged data, probably because the data were already binned into weekly averages and the response time for phytoplankton to nutrient inputs in Monterey Bay generally occurs on shorter time scales (e.g., <4 days, as shown from the aerosol addition experiment in this study). Therefore, at least part of the growth responses to aerosol additions was likely captured during the same week-long period as the deposition event occurred and therefore did not show a stronger correlation using a 1 week lag.

[35] However, because regression analysis cannot prove a causal relationship between two data sets that covary, it is possible that the covariance of AOT and Chl *a* was due to their mutual dependence on a third variable. For example, higher wind speeds would be expected to bring more aerosol

Table 2. Depositional Fluxes of N From Fine and Coarse Fractions in Summer and Winter

	NO_x (μg N m^{-2} d^{-1})		NH_4 (μg N m^{-2} d^{-1})	
Aerosol Season and Fraction	Range	Mean ± SE	Range	Mean ± SE
Summer coarse	29–220	76 ± 13	10–81	27 ± 5
Winter coarse	20–128	80 ± 8	4–72	32 ± 8
Summer fine	3–48	11 ± 3	4–22	9 ± 1
Winter fine	4–52	24 ± 4	8–52	24 ± 4

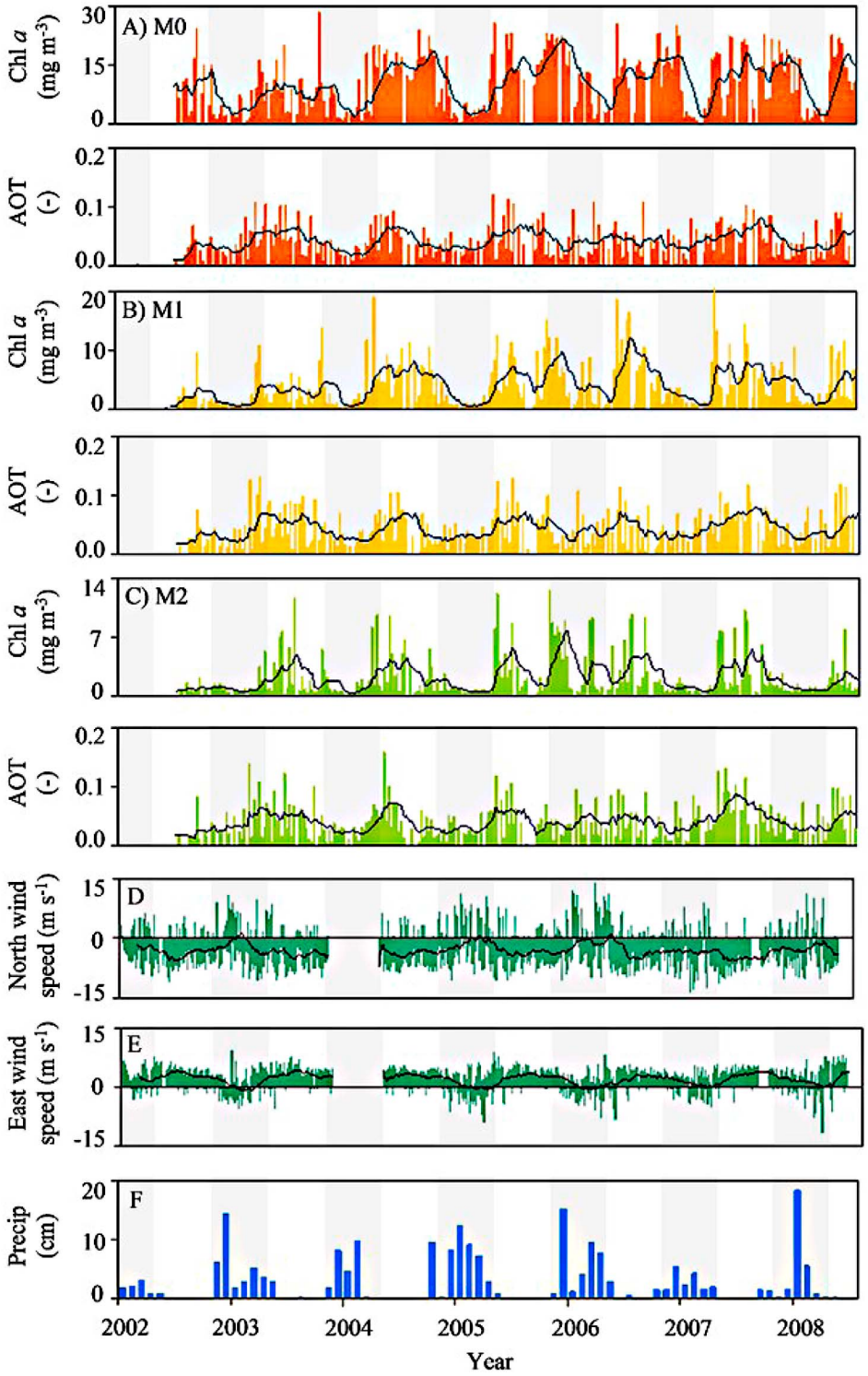

Figure 5. Time series of MODIS-derived weekly averaged AOT and Chl *a* levels for stations (a) M0, (b) M1, and (c) M2 between 2002–2008, along with (d) zonal and (e) meridional components of wind velocity at station M2, and (f) monthly precipitation at Pinnacles National Monument in San Benito County, California. Shaded regions denote winter. Trend lines show 2 month moving averages.

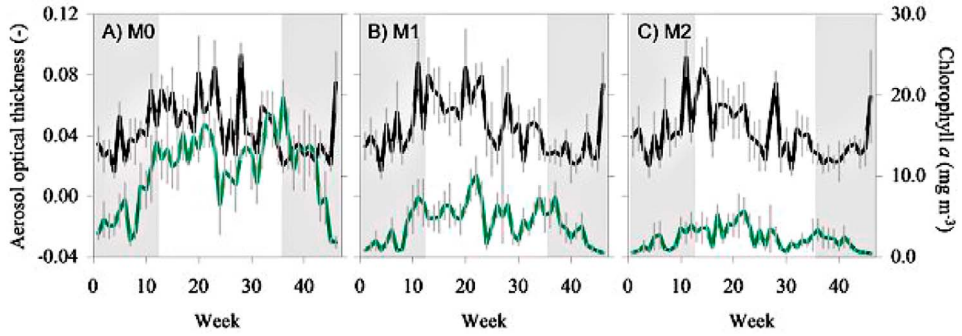

Figure 6. Annual time series for MODIS-derived aerosol optical thickness and Chl *a* for station (a) M0, (b) M1, and (c) M2. Data points are averages for each week from 2002–2008, error bars show standard error of the mean, and shaded regions denote winter weeks.

particles but would also potentially cause more upwelling. To test if the correlation between AOT and Chl *a* existed during periods when the nutricline is suppressed and deep-water nutrients are less abundant, we performed the regression using data only from El Niño periods during the record (Figure 8). Significant relationships were identified for all three stations during El Niño periods (Table 3), where AOT accounted for 0.1%, 4.3%, and 11.3 % of the variance in Chl *a* levels at stations M0, M1, and M2, respectively.

3.4. Phytoplankton Growth Experiments

[36] Culture experiments with phytoplankton isolated from coastal California showed similar positive growth with NO_3 and with natural aerosol particles collected near Monterey Bay (Figure 9). While growth was not significantly different ($p < 0.05$) between treatments for each strain at all time points during the 6 day experiment, it appears that growth of *Thallasiosira* and *Synechococcus* 2515 cultures receiving particulate aerosols was beginning to decline by day 6. *Synechococcus* 1284 showed a ~3 day lag period in replicates receiving NO_3, whereas the lag period was ~4 days in all replicates receiving particulate aerosols as the sole source of N.

[37] Natural phytoplankton assemblages from Monterey Bay were also able to grow using N from particulate aerosols. The dinoflagellates *Ceratium furca* and *Ceratium divaricatum var. balechii* accounted for the vast majority of phytoplankton cells in our sample water, although smaller populations of *Pseudo-nitzschia australis* were also observed. At the start of the incubation, the baseline Chl *a* level was 26 mg m^{-3}, and after 30 h, the control (25 mg m^{-3}) was not statistically different ($p < 0.05$) than baseline (Figure 10). In contrast, Chl *a* increased significantly relative to control and baseline levels in the other treatments, reaching 40 mg m^{-3} in the nitrate treatment and 34 mg m^{-3} in the particulate aerosol treatment.

4. Discussion

4.1. Atmospheric Deposition of N in Coastal California

[38] Seasonally weighted particulate aerosol concentrations (total suspended particle, TSP) at Monterey Bay ranged from 14 to 160 μg m^{-3} (Table 1) and were similar to values reported for other terrestrial sites within northern [*Wells et al.*, 2007; *John et al.*, 1973; *Herner et al.*, 2005] and southern California [*Chow et al.*, 1994], but were 1–2 orders of magnitude more concentrated than over the open Pacific Ocean [*Uematsu et al.*, 1983]. The annual dry deposition rates based on our data (24 and 34 mg m^{-2} d^{-1} for winter and summer, respectively; Table 1) were 2-fold to

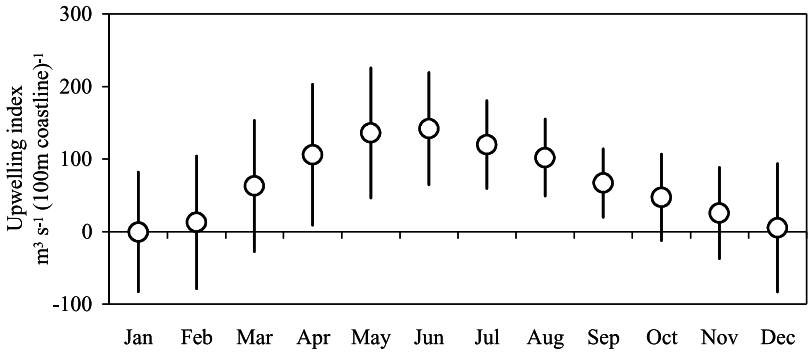

Figure 7. Monthly averaged values of upwelling indices for the period of record 1962–2008. Error bars show standard deviation.

Table 3. Regression Statistics for MODIS-Derived Chl *a* and AOT Data for Monitoring Stations M0, M1, and M2[a]

	M0			M1			M2		
	n	R^2	*p*	*N*	R^2	*p*	*n*	R^2	*p*
Summer	125	0.2%	0.650	125	3.9%	**0.028**	122	6.6%	**0.004**
Winter	97	<0.1%	0.975	99	2.2%	0.145	97	2.2%	0.147
El Niño	148	0.1%	**0.006**	150	4.3%	**0.011**	146	11.3%	**<0.001**

[a]The correlation is significant ($p < 0.05$, shown in bold typeface) in the summer weeks for stations M1 and M2 and during El Niño periods for all three stations. No significant correlations were found for any of the stations in the winter weeks.

10-fold higher than modeled average deposition rates for the region (~1.4–14 mg m^{-2} d^{-1}) [*Mahowald et al.*, 2005], likely because the model also integrates low concentration TSP measurements from the open Pacific Ocean [*Uematsu et al.*, 1983].

[39] In summer, winds generally traveled southeast along the coast before reaching Monterey Bay (Figures 2, 5d, and 5e). Summer particulate aerosol samples traversing open water contained less soluble N and P but higher proportions of sea salts (Table 1), whereas in winter, when westward winds were more common (Figures 2a and 5e), concentrations of soluble N and P were higher, possibly owing to more frequent overland trajectories that incorporate more nutrient-rich crustal and anthropogenic material [*Sadasivan*, 1978]. Our particulate aerosol nitrate plus nitrite (NO_x, 0.14–1.2 μg N m^{-3}) and NH_4 (0.11–1.2 μg N m^{-3}) concentrations were on the low end of published ranges for terrestrial sites in California [*Herner et al.*, 2005], likely because our coastal site is more removed from anthropogenic N sources. As would be expected from particulate aerosols collected closer to land, NO_x and NH_4 concentrations were approximately an order of magnitude higher in our samples than in those collected over the Pacific Ocean [*Parungo et al.*, 1986; *Quinn et al.*, 1990; *Buck et al.*, 2006]. Soluble Fe ranged from 1.7 to 10.7 ng m^{-3} in summer and from 4.3 to 15.3 ng m^{-3} in winter and was slightly higher than for samples collected from the North Pacific subtropical gyre [*Buck et al.*, 2006].

[40] Aerosol particle addition as a sole source of N in laboratory experiments stimulated growth of cyanobacteria and diatoms (Figure 9). Moreover, natural populations showed increased Chl *a* following nitrate and particulate aerosol additions (Figure 10). The dominant species in our incubation, *C. furca* and *C. divaricatum var. balechii*, are both common bloom formers that are observed frequently in Monterey Bay [*Ryan et al.*, 2008]. The increased growth and Chl *a* observed in these experiments suggest that N in dry deposition is bioavailable to phytoplankton present in coastal California water.

[41] To determine the contribution of N from atmospheric deposition to overall new production in this region, we calculated the combined input of NO_x and NH_4 from aerosol particles <10 μm using calculated deposition rates and the representative mixed layer depth for each season. For these estimates, we define atmospheric deposition here as wet plus dry deposition (excluding deposition of gases) and assume that all of the soluble NO_x and NH_4 are used by phytoplankton and that none is removed by bacteria or other processes. These calculations indicate that dry deposition provides 123 μg N m^{-2} d^{-1} in summer and 164 μg N m^{-2} d^{-1} in winter. A seasonally weighted average gives a dry deposition supported new production estimate of 133 μg N m^{-2} d^{-1} or 10.3 μg N m^{-3} d^{-1}, assuming mixing depths of 10 and 40 m in the summer and winter, respectively [*Olivieri and Chavez*, 2000]. Wet deposition during the winter months contributes an additional 79 μg N m^{-2} d^{-1} (2.0 μg N m^{-3} d^{-1}), giving a combined deposition (dry plus wet) of 213 μg N m^{-2} d^{-1} (12.3 μg N m^{-3} d^{-1}). Compared to estimates of new production for Monterey Bay under average annual conditions [*Kudela and Chavez*, 2000, Table 4], atmospheric deposition of N to offshore waters provides 0.11%–0.24%

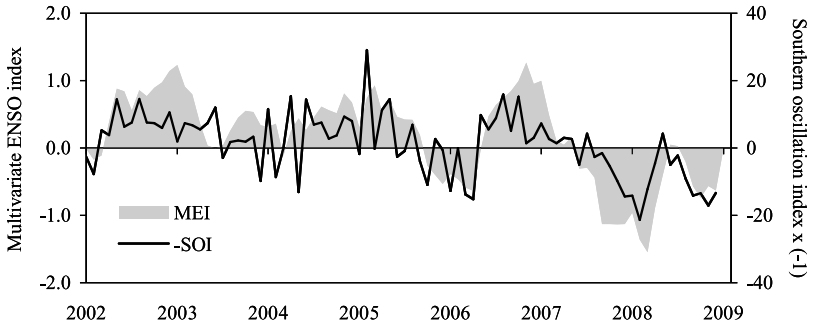

Figure 8. ENSO indices for 2002–2008. Positive MEI values and negative SOI values indicate El Niño periods. In the figure SOI values have been multiplied by −1 to facilitate comparison with MEI values such that positive values on both scales indicate periods of El Niño.

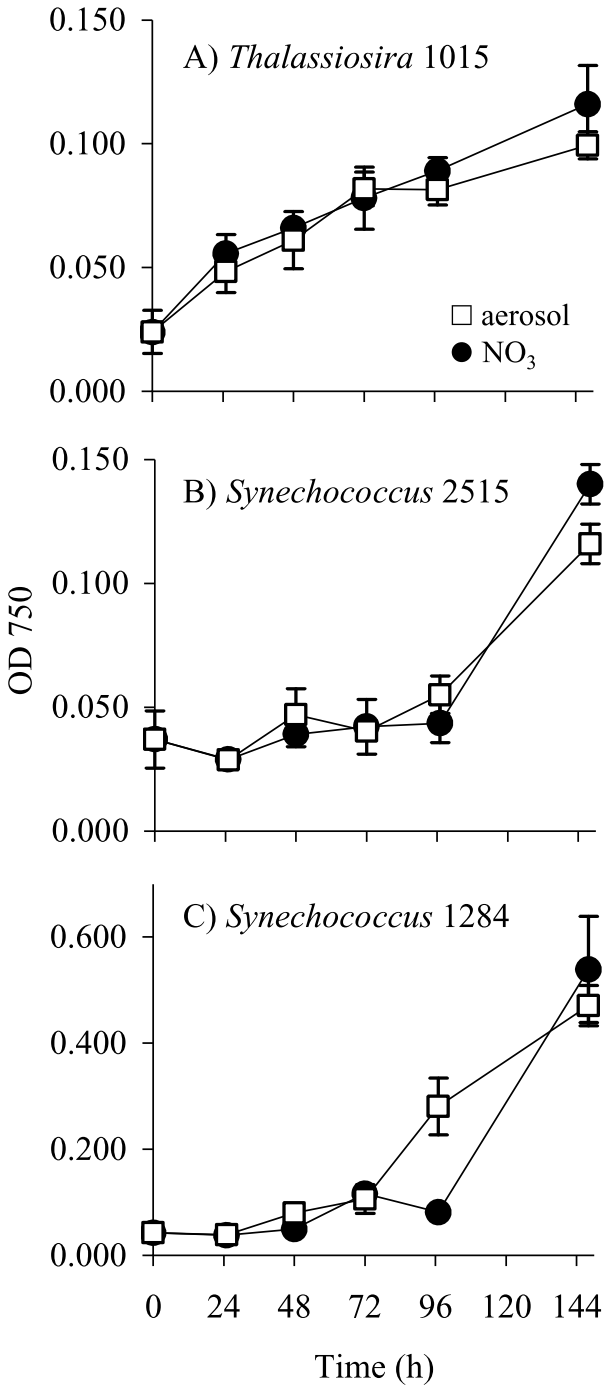

Figure 9. Growth of cultured phytoplankton strains isolated from coastal California on F/2-NO_3 media with either NO_3 (filled circles) and aerosol derived N (open squares). Error bars show SE and are contained within the symbol when not visible.

of new N on an annual basis. We note that these are minimal estimates because they are based on NH_4 and NO_x and do not include other forms of bioavailable N present in atmospheric deposition. For example, if gaseous N, which we did not measure directly, is important [*Kouvarakis et al.*, 2001], we may be underestimating the N input. Similarly, organic N may account for ~30% of atmospheric N [*Cornell et al.*, 1995; *Peierls and Paerl*, 1997; *Cornell et al.*, 2003], of which 20%–30% is bioavailable to marine phytoplankton [*Peierls and Paerl*, 1997]. If atmospheric deposition in coastal California contains similar proportions of bioavailable organic N deposition (e.g., an additional 91 μg N m^{-2} d^{-1}, of which 18–27 μg N m^{-2} d^{-1} is bioavailable), then atmospheric deposition of N to offshore waters would provide up to 0.12%–0.27% of new N on an annual basis.

[42] Atmospheric N deposition (including organics) would support productivities of 0.8 mg C m^{-2} d^{-1} in the summer and 1.5 mg C m^{-2} d^{-1} in the winter, based on average deposition rates and assuming a Redfield C/N ratio of 106:16. We note that natural variability exists in phytoplankton elemental stoichiometries. C/N ratios as low as ~4.5 have been observed in Monterey Bay [*Kudela and Dugdale*, 2000], although most phytoplankton C/N ratios are less than 8.7 during balanced growth [*Geider and LaRoche*, 2002]. Our estimates could therefore potentially overestimate or underestimate the amount of productivity by ~25%. The Redfield value we use represents a midrange value for C/N and is also consistent with the assumptions used by *Kudela and Chavez* [2000] to estimate overall new production in Monterey Bay that we use in Table 4.

[43] Although, on an annual average, N in atmospheric deposition contributes a small portion of new production, the role may be more significant during nonupwelling periods. The particulate aerosol NO_x/P ratios in our particulate aerosol samples (Figure 4) were approximately an order of

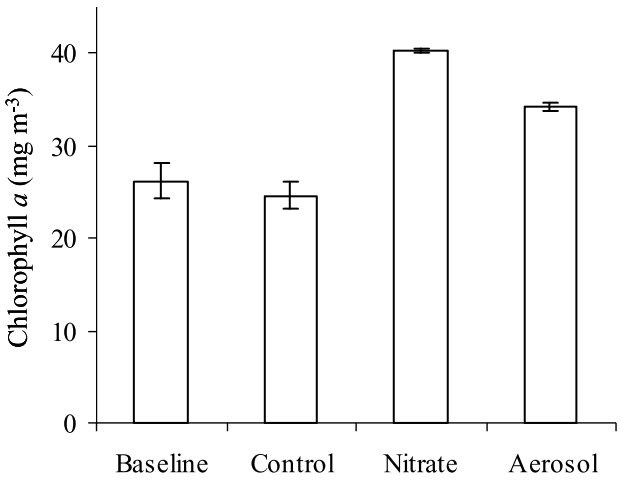

Figure 10. Chlorophyll *a* levels from an incubation experiment with natural phytoplankton assemblages in Monterey Bay. Bars show mean Chl *a* concentration at baseline before additions were made, and after 30 h of incubation for the control, nitrate, and aerosol treatments. Error bars show standard error.

Table 4. Productivity Supported by Aerosol N[a]

	New N Production[b] (mg N $m^{-3}d^{-1}$)	New Production From Atmospheric N During High-Deposition Events	New Production From Atmospheric N Based on Mean Annual Deposition Rates	New Production From Dry Deposition of Fe
M2, annual	5.04	0.5%	0.2%	–
M2, upwelling	15.4	0.2%	0.08%	1.9%
M2, El Niño	1.96	1.3%	0.6%	–
M2, low productivity[c]	0.06	50%	13.5%	–
M1, annual	11.06	0.2%	0.1%	–
M1, upwelling	29.12	0.1%	0.04%	1.0%
M1, El Niño	3.22	0.8%	0.4%	–
M1, low productivity	0.14	20%	9%	–

[a]Estimates show the percentage of new production attributable to aerosol-derived N on high deposition days, N derived from mean wet and dry deposition combined, and aerosol Fe based on mean nutrient flux data from extracted aerosol samples during annual, upwelling, El Niño, and low-productivity periods for Monterey Bay.
[b]Total new production values for Monterey Bay are from *Kudela and Chavez* [2000].
[c]Values for M2 low productivity are not available. We assumed the same proportion between annual and low productivity as for M1.

magnitude greater than the ratio required for phytoplankton growth (16N:1P). Complete utilization of N from particulate aerosols is likely during nonupwelling periods, when productivity in Monterey Bay is N limited [*Kudela and Dugdale*, 2000]. Moreover, N input may increase substantially when large deposition events occur (e.g., the mean depositional flux of PM10 aerosols for summer was 34 ± 2 mg m^{-2} d^{-1}, whereas the maximum flux was 89 mg m^{-2} d^{-1}, approximately 2.6-fold higher than the average.) Atmospheric deposition therefore could support 9% of new production during low productivity winter days with average deposition rates and potentially up to 20% of new production when dry deposition is maximal (Table 4). Primary production in Monterey Bay also varies substantially from day to day depending on season [*Pennington and Chavez*, 2000] and is as low as 20–50 mg C m^{-2} d^{-1} during nonupwelling periods [*Bac et al.*, 2003]. Atmospheric deposition could therefore support up to 7.5% of primary production during such low-productivity days but could be up to 13% of primary production on days with high deposition and no nutrient input from upwelling.

[44] During upwelling events, production rates increase dramatically, reaching over 1000 mg C m^{-2} d^{-1} [*Bac et al.*, 2003; *Pennington and Chavez*, 2000]. Clearly atmospheric N deposition (mostly dry deposition during the spring and summer) would support only a minor component of total primary production during upwelling periods. However, similar to some high-N low-chlorophyll (HNLC) regions [*Martin and Fitzwater*, 1988; *Coale et al.*, 1996; *Boyd et al.*, 2000], there is compelling evidence that primary production at such times is limited by Fe rather than N along some sections of the California coast. For example, during the summer and fall upwelling sustains elevated nitrate levels while iron is drawn down along parts of the coast [*Johnson et al.*, 2001; *Chase et al.*, 2005]. Shipboard iron addition experiments conducted with seawater collected from geochemically diverse regions along the California coast showed Fe limitation was stronger offshore in waters away from sediment sources and in aged upwelled water [*Firme et al.*, 2003]. Phytoplankton community composition can also be affected by Fe limitation; incubations using nanomolar additions of Fe to nearshore waters promoted blooms of chain forming diatoms and resulted in the complete drawdown of seawater nitrate in coastal California waters [*Hutchins and Bruland*, 1998].

[45] Typical upwelled water brings 20 μmol L^{-1} NO_3 to the surface ocean in coastal California [*Pennington and Chavez*, 2000]. Assuming a cellular Fe/C ratio of 20 μmol Fe/mol C [*Sunda and Huntsman*, 1995; *Bruland et al.*, 2001] and a Redfield C/N ratio, phytoplankton would require ~133 μmol Fe/mol N [*Bruland et al.*, 2001]. The average flux of soluble Fe in our samples (1.5 μg m^{-2} d^{-1}) could therefore support an uptake of 2.9 mg N m^{-2} d^{-1} (0.29 mg m^{-3} d^{-1} assuming a 10 m mixed depth) or the equivalent of ~ 1.9% of new production at offshore stations M2, during high-productivity upwelling periods (Table 4). On days with high dry deposition, the Fe supplied could support up to 5% of new production during the upwelling period. A more conservative Fe/C ratio of 40 μmol Fe/mol C [*Martin and Knauer*, 1973, *Bruland et al.*, 2001] would indicate that Fe from dry deposition could support ~0.5%–1% of new production at stations M1 and M2, respectively, suggesting that even if luxury uptake of Fe occurs [*Sunda and Huntsman*, 1995], dry deposition may still contribute to new production and possibly impact species abundance and their nutritional requirements in coastal California [*Hutchins and Bruland*, 1998; *Bruland et al.*, 1991; *Takeda*, 1998]. We note that these are minimal estimates, as wet deposition of Fe has not been accounted for in our study and may contribute significant Fe [*Duce and Tindale*, 1991].

4.2. Aerosol and Chlorophyll Relationship Based on Remote Sensing

[46] The calculations of the contribution of dry deposition to new production in coastal California presented above are based on a relatively small data set of particulate aerosol samples collected from June 2008 through January 2009. To determine how these data fit within the longer-term trends, we used remote sensing data of aerosol optical thickness (AOT) and chlorophyll *a* (Chl *a*) from the past 6 years (the entire MODIS data set; Figures 5a–5c). Assuming our data of particulate aerosol chemistry is representative, we see that despite higher N, P, and Fe concentrations in winter, no

Table 5. Aerosol Concentration, N Content, Deposition Rate, and Contribution to Total Primary Production in Coastal California and Six Other Major Upwelling Regions Throughout the World's Oceans: The NW and SW Coasts of Africa, the SE Coast of the Arabian Peninsula Near the Somali Coast, the West Coast of India, the West Coast of Australia, and the West Coast of South America[a]

Ocean Basin	Location	Longhurst Upwelling Province[b]	Aerosol Concentration-TSP (μg aerosol/m^3)	NO^3 Aerosol Concentration (μg N/m^3)	NH4 Aerosol Concentration (μg N/m^3)	Total Soluble N (μg N/m^3)	Dust Deposition Rate[c] (g aerosol/m^2/yr)	Aerosol-Derived Productivity[d] (g C/m^2/yr)	Annual Primary Production[b] (g C/m^2/yr)	Portion of Annual Productivity From Aerosols (%)	References for Aerosol Chemistry Data
Pacific	West Coast of USA, Crater Lake, and Mt. Lassen	Coastal California (CCAL)	7.3								*VanCuren* [2003]
Pacific	West Coast of USA, Crater Lake, Mt. Rainier, Mt. Lassen, and Cheeka Peak	Coastal California (CCAL)	2.04–3.91								*Jaffe et al.* [2005]; PM2.5 only
Pacific	California, Sequoia National Park	Coastal California (CCAL)	1–30								*Wells et al.* [2007]; PM10 soil
Pacific	West Coast of USA, 30°N–40°N, 125°W	Coastal California (CCAL)	9.4–17	0.041–0.0565	0.078–0.101						*Parungo et al.* [1986]
Pacific	West Coast of USA, 20°N–29°N	Coastal California (CCAL)	8.9–13	0.020–0.050	0.039–0.058						*Parungo et al.* [1986]
Pacific	West Coast of USA, open ocean to coastal	Coastal California (CCAL)		0.068–0.160							Savoie (1984) in *Duce et al.* [1991]
Pacific	Sub-Arctic NW Pacific Ocean Station Papa (50°N, 145°W)	Coastal California (CCAL)	3.7	0.131	0.07						*Phinney et al.* [2006]; particles diameter > 0.8 μm
Pacific	North Pacific Subtropical Gyre, Midway, Oahu, Enewetak, and Fanning Islands	Coastal California (CCAL)	0.06–0.84								*Uematsu et al.* [1983]; range of averages
Pacific	Northwest Pacific Ocean and North Pacific Subtropical Gyre near Hawaiian Islands	Coastal California (CCAL)		0.014–0.280							*Buck et al.* [2006]
Pacific	North Pacific, 30°N–50°N, 170°W	Coastal California (CCAL)			0.482–1.400						*Quinn et al.* [1990]
Pacific	North Pacific, 15°N–29°N, 170°W	Coastal California (CCAL)			0.187–0.327						*Quinn et al.* [1990]
Pacific	Equatorial Pacific, 11°N–14°N, 170°W	Coastal California (CCAL)			0.109–0.389						*Quinn et al.* [1990]
Pacific	San Francisco Bay area, Pittsburg, Richmond, San Rafael, San Francisco, Burlingame, Redwood City, San Jose, Fremont, and Livermore	Coastal California (CCAL)	43–166								*John et al.* [1973]; values represent measurements made over 1 day in summer
Pacific	San Joaquin Valley; Davis, Modesto, Sequoia, and Bakersfield	Coastal California (CCAL)	5–185	0.226–20.323	0.778–31.111						*Herner et al.* [2005]
Pacific	West Coast of California, Bodega Bay	Coastal California (CCAL)	20–270	0.226–5.645	0.778–10.111						*Herner et al.* [2005]
Pacific	Los Angeles, CA, Summer; Burbank, downtown LA, Hawthorne, Long Beach, Anaheim, Rubidoux, San Nicolas Island, Azusa, and Claremont	Coastal California (CCAL)	45.9–120	0.357–6.512	0.661–6.689						*Chow et al.* [1994]; range of averages for all sites
Pacific	Los Angeles, CA, Fall; Burbank, downtown LA, Hawthorne, Long Beach, Anaheim, and Rubidoux	Coastal California (CCAL)	85.1–104	4.785–7.969	4.947–8.042						*Chow et al.* [1994]; range of averages for all sites
Pacific	MBARI	Coastal California (CCAL)	14–160	0.138–1.219	0.109–1.244						This work, NO^3 includes NO^2
	"Midrange" values	Coastal California (CCAL)	**20**		**1**		**5**	**1.4**	**388**	**0.4**	
Atlantic	Izana, Tenerife, Canary Islands	NW Africa (CNRY)	22.28	0.174	0.257						,
Atlantic	Sal Island, Cape Verde Archipelago	NW Africa (CNRY)	5–120								*Chiapello et al.* [1995]
Atlantic	NW African coast 0°N–20°N	NW Africa (CNRY)				0.14–0.91					*Baker et al.* [2006]
Atlantic	Central South Atlantic Ocean	NW Africa (CNRY)				0.21–1.12					*Baker et al.* [2006]
Atlantic	Central North Atlantic Ocean, Transect from Dakar to Azores	NW Africa (CNRY)		0.034–0.309	0.061–0.619						*Church et al.* [1991]
Atlantic	Tropical North Atlantic, Transect between Barbados and Cape Verde	NW Africa (CNRY)	0.8–55.6	<0.054–0.298	0.053–0.233						*Johansen et al.* [2000]
Atlantic	Near African coast	NW Africa (CNRY)	57								*Chester et al.* [1972]
Atlantic	SE of Cape Verde	NW Africa (CNRY)	133								*Chester et al.* [1972]
Atlantic	Sal Island, Cape Verde Archipelago	NW Africa (CNRY)	29.8								*Savoie and Prospero* [1977]
Atlantic	NW African coast, Canary Islands	NW Africa (CNRY)		0.271							Savoie (1984) in *Duce et al.* [1991]

Table 5. (continued)

Ocean Basin	Location	Longhurst Upwelling Province[b]	Aerosol Concentration-TSP (μg aerosol/m^3)	NO^3 Aerosol Concentration (μg N/m^3)	NH4 Aerosol Concentration (μg N/m^3)	Total Soluble N (μg N/m^3)	Dust Deposition Rate[c] (g aerosol/m^2/yr)	Aerosol-Derived Productivity[d] (g C/m^2/yr)	Annual Primary Production[b] (g C/m^2/yr)	Portion of Annual Productivity From Aerosols (%)	References for Aerosol Chemistry Data
Atlantic	NW African coast, Equatorial Atlantic	NW Africa (CNRY)		0.16							Savoie (1984) in *Duce et al.* [1991]
Atlantic	Near the ITCZ	NW Africa (CNRY)	0.25								*Chester et al.* [1972]
	"Midrange" values	NW Africa (CNRY)	**30**		**0.1**		**50**	**0.95**	**732**	**0.1**	
Indian	NW Indian Ocean	Arabian Peninsula/ West India (ARAB/INDW)	1–7.6	0.097–0.228							*Savoie et al.* [1987]
Indian	NW Indian Ocean	Arabian Peninsula/ West India (ARAB/INDW)	0.4–3.9	0.067–0.452	0.156–1.167						*Krishnamurti et al.* [1998] range of stations 9–31
Indian	NW Indian Ocean	Arabian Peninsula/ West India (ARAB/INDW)	<0.1	0.228	0.187						*Rhoads* [1998]; NHmE region
Indian	Arabian Sea	Arabian Peninsula/ West India (ARAB/INDW)	25								
Indian	Somali Coast	Arabian Peninsula (ARAB)	0.23	0.038							*Savoie et al.* [1987]
Indian	Arabian Sea, Arabian Peninsula and Somali Coast	Arabian Peninsula (ARAB)		0.149							Savoie (1984) in *Duce et al.* [1991]
Indian	Arabian Sea along West India Coast	West India (INDW)	4.7–18.4	0.587–1.852	1.011–4.589						*Krishnamurti et al.* [1998]; range of stations 32–35
Indian	Arabian Sea along West India Coast	West India (INDW)		0.075							Savoie (1984) in *Duce et al.* [1991]
Indian	Arabian Sea	West India (INDW)	6.2	0.386	0.552						*Rhoads* [1998]; NHcT region
	"Midrange" values	Arabian Peninsula (ARAB)	**2**		**0.6**		**20**	**34**	**454**	**8**	
	"Midrange" values	West India (INDW)	**5**		**1**		**20**	**23**	**369**	**6**	
Indian	Bay of Bengal	West Australia (AUSW)	7.2								*Prospero* [1979]
Indian	Equatorial Indian Ocean 50°E–100°E	West Australia (AUSW)	<0.1	0.05	0.062						*Rhoads* [1998]; SHmE region
Indian	Amsterdam Island	West Australia (AUSW)	0.12								*Ezat and Dulac* [1995]
Indian	Amsterdam Island, KEOPS cruise	West Australia (AUSW)	0.013								*Wagener et al.* [2008]
Indian	Cape Grim, Tasmania, Australia	West Australia (AUSW)		0.034	0.028						*Mace et al.* [2003]
Indian	East Indian Ocean	West Australia (AUSW)		0.020–0.140							Savoie (1984) in *Duce et al.* [1991]
	"Midrange" values	West Australia (AUSW)	**1**		**0.09**		**5**	**2.6**	**199**	**1**	
Atlantic	Central South Atlantic	SW Africa (BENG)	0.3	<0.002	0.047						*Zorn et al.* [2008]
Atlantic	SW African coast 30°S–40°S	SW Africa (BENG)	2.18	0.009	0.14						*Zorn et al.* [2008]
Atlantic	SW African coast 0°S–20°S	SW Africa (BENG)				0.14–0.35					*Baker et al.* [2006]
Atlantic	SW African coast, open ocean to coastal	SW Africa (BENG)		0.02							Savoie (1984) in *Duce et al.* [1991]
	"Midrange" values	SW Africa (BENG)	**1**		**0.001**		**20**	**0.11**	**323**	**0.04**	
Pacific	Chilean coast, Chillan	West South America (CHIL)	83.4	2.296	4.107						*Celis et al.* [2004]
Pacific	Chilean coast, 30°S transect from La Serena to Cerro Tololo	West South America (CHIL)	6.4–55.2								*Fiebig-Wittmaack et al.* [2006]
Pacific	Chilean coast, urban cities Temuco, Rancaua, Valparaiso, Iquique, Viña del Mar	West South America (CHIL)	55.5–77.6								*Kavouras et al.* [2001]; for PM10
Pacific	West South America, open ocean to coastal	West South America (CHIL)		0.02							Savoie (1984) in *Duce et al.* [1991]
	"Midrange" values	West South America (CHIL)	**50**		**0.1**		**10**	**0.11**	**269**	**0.04**	

[a]We used midrange values of aerosol concentration (TSP) and N content, along with modeled aerosol deposition rates [*Mahowald et al.*, 2005] to estimate annual N deposition in each region. We compared the productivity supported by these N additions (assuming a Redfield ratio of 106C:16N) to modeled estimates of annual productivity for each region [*Longhurst et al.*, 1995]. These estimates provided an order of magnitude approximation for the fraction of productivity in each region that is supported by aerosol N deposition.

[b]Geographical provinces and primary productivity values were obtained from *Longhurst et al.* [1995].

[c]Dust deposition rates obtained from *Mahowald et al.* [2005].

[d]Aerosol-derived productivity was calculated as the product of aerosol concentration (μg aerosol m^{-3} air), aerosol N content (μg aerosol m^{-3} air), and aerosol deposition rate (g aerosol m^{-2} yr^{-1}). A Redfield C/N ratio of 106:16 was assumed to convert from N deposition to C production.

significant correlations were found between AOT and Chl *a* for any of the stations during the winter ($p < 0.05$; Table 3). This is consistent with our calculated inputs of new N from dry deposition, which were lower in winter than summer on a per volume basis because the nutrients get distributed over a deeper mixed layer in winter. In addition, nutrient inputs from precipitation and fluvial discharge increase dramatically in the winter (Figure 5f), contributing a larger proportion of new nutrient inputs along the coast that are likely bioavailable to phytoplankton [*Peierls and Paerl*, 1997]. Specifically, wet deposition during the winter months contributes an additional 79 μg N m^{-2} d^{-1} or ~50% additional N than from dry deposition alone (164 μg N m^{-2} d^{-1}). Aerosol dry deposition therefore contributes a smaller relative portion of new nutrients during the winter, when wet deposition occurs, than in the summer when wet deposition is minimal. Because wet deposition is not reflected in the AOT data, rainfall may contribute to the lack of significant correlation between AOT and Chl *a* during the winter. This effect is most pronounced at the coastal site M0, where nutrient input from perennial river discharge and runoff also serve to obscure any relation between AOT (dry deposition) and Chl *a*.

[47] In contrast, significant correlations between AOT and Chl *a* were observed for stations M1 and M2 in summer ($p < 0.05$; Table 3). Coastal upwelling is an episodic, wind-driven event that occurs on the order of days and then relaxes and, in Monterey Bay, is more frequent during May through July than the rest of the summer [*Kudela and Chavez*, 2000; *Olivieri and Chavez*, 2000, Figure 7]. The significant AOT-Chl *a* correlation during the summer could therefore be due to cooccurrence of high-aerosol particle loads and large deep-water nutrient input from strong upwelling (e.g., both brought by strong winds) or could indicate a real causal relationship between dry deposition and Chl *a* that is sustained throughout the summer.

[48] During El Niño periods, the nutricline is suppressed along the California coast, restricting intrusion of nutrients from deep water into the euphotic zone [*Kudela and Chavez*, 2000]. Indeed, global decreases in primary production have been observed following transitions between La Niña and El Niño periods [*Behrenfeld et al.*, 2006]. AOT levels were not statistically different between El Niño and La Niña years during our period of record ($p < 0.05$). This suggests that in contrast to the Atlantic Ocean, where the North Atlantic Oscillation (NAO) is significantly correlated with AOT over the Mediterranean Sea and African coast [*Moulin et al.*, 1997], aerosol particle concentrations along the coast of California may not be strongly influenced by interannual climate cycles (though other physical processed like upwelling and rainfall are clearly influenced).

[49] Within our data set, significant relationships between AOT and Chl *a* were identified for all stations during El Niño periods ($p < 0.05$; Table 3). In addition, the trend indicates that the importance of dry deposition as a nutrient source increased with distance offshore (Table 3). On the basis of new production estimates for Monterey Bay during El Niño periods [*Kudela and Chavez*, 2000] (Table 4), dry deposition contributes 0.32%–0.53% of new N during El Niño periods. While this is still a relatively small amount, it is over twice the amount as when all years are considered. When wet deposition is included, the contribution to new production is approximately 20%–40% greater than for dry deposition alone (e.g., wet N deposition during La Niña periods ranged from 47 to 90 μg N m^{-2} d^{-1}, whereas it ranged from 69 to 112 μg N m^{-2} d^{-1} during and leading into El Niño periods (Table 4)).

[50] At the coastal station M0, almost no variability in Chl *a* could be attributed to AOT during any season or ENSO condition (Table 3), consistent with long-term monitoring that indicates nearshore sites receive more nutrients from anthropogenic inputs, runoff, and fluvial discharge than offshore waters. Therefore, it is possible that carryover of nutrients from nearshore processes and efficient nutrient recycling is sufficient to support phytoplankton growth close to shore even during El Niño periods, whereas phytoplankton in offshore waters, which are still within the coastal zone but further removed from these nutrient sources, may depend more on nutrients from atmospheric deposition.

[51] While suppression of the nutricline during El Niño summers serves to increase the relative contribution of N from dry deposition, increased wet deposition and river discharge during El Niño winters would have the opposite effect. In our overall winter data set, we observed no significant relationship between AOT and Chl *a* during winter months, particularly close to shore where inputs from runoff and river discharge are more concentrated. During El Niño winters, this effect is likely to be even larger. For example, during the anomalously strong El Niño conditions in winter and early spring of 1998, a 5-fold increase in Chl *a* was observed that extended from nearshore to 300 km offshore [*Kudela and Chavez*, 2004]. These observations were attributed to input from the San Francisco Bay outflow, which introduced nitrate levels similar to upwelling conditions (ca. 30 μM) close to shore [*Friederich et al.*, 2002; *Wilkerson et al.*, 2002]. In such extreme El Niño winters, dry deposition would play a negligible role, although the wet deposition role will increase. The greatest impact from atmospheric dry deposition during El Niño periods would be likely to occur offshore in the summer, when fluvial inputs are minimal, precipitation is negligible (Figure 5f), and nutrient input from deep water is suppressed. The possible transition to extended or permanent El Niño conditions in response to climate warming-induced ocean stratification [*Wara et al.*, 2005; *Sarmiento et al.*, 2004] may therefore increase the proportion of productivity supported in summer by dry deposition and in winter by wet deposition for coastal California and possibly other upwelling regions.

4.3. Role of Dry N Deposition in Coastal Upwelling Regions

[52] To get an order of magnitude approximation for the amount of productivity that is supported by dry deposition of N in other major upwelling regions, we calculated new production values based on dry N deposition for six other locations. The particulate aerosol concentration and N content values used in the calculations were based on midrange published data and were calculated based on annual average productivity and deposition rates (Table 5).

On the basis of these estimates, dry N deposition supports between 0.04%–8% of productivity throughout the world's coastal upwelling regions. The estimate for the California coast, based on published data for central and northern California (0.4%), is within the same range as the values calculated directly from our measured data (~0.1%–0.5%, Table 1). The estimate of productivity from dry N deposition for the northwest coast of Africa is also within this range (~0.1%). Similar to the North America upwelling region, the northwest coast of Africa is highly productive due to substantial upwelling events, though dry deposition is roughly an order of magnitude greater and N content is an order of magnitude lower, likely due to fewer anthropogenic N contributions to the dominant Sahara dust.

[53] The most substantial contribution of dry deposition to productivity occurs in the Indian Ocean along the Arabian Peninsula (8 %) and the west coast of India (6%), where dry deposition is very high. Notably, the effect of total atmospheric deposition could be considerably higher, particularly during the monsoon season. The estimated productivity from dry N deposition for the west coast of Australia (1%) is lower than for the other Indian Ocean regions but agrees with satellite observations that aerosol optical thickness is generally lower than would be expected based on Australia's large desert. Perhaps not surprisingly based on their location in the Southern Hemisphere where aeolian particles are scarce, the southwest coast of Africa (0.04%) and the west coast of South America (0.04%) have the lowest estimates of productivity from dry N deposition among the seven major upwelling regions.

[54] As with N deposition in coastal California, the input of N from dry deposition in these regions may be more important during large deposition events and/or during nonupwelling periods. However, this level of detail is not possible to quantify based on the annually averaged values used in our calculations; higher-resolution deposition and primary productivity data would be needed to quantify the role of dry deposition during these shorter periods. Moreover, our calculations may underestimate the actual percentage because they do not account for all bioavailable forms of N present in dry deposition (only NH_4 and NO_3 are considered) and do not consider the potential fertilizing effects of other nutrients (specifically Fe). Increased new production resulting from stimulation of N_2 fixation by nutrients in dry deposition [*Mills et al.*, 2004] is also neglected in these calculations. As noted above, inclusion of wet deposition in these estimates would likely increase the N inputs by 40%–100% [*Herut et al.*, 1999; *Nadim et al.*, 2001], roughly doubling our estimates of the percentage of productivity supported by N deposition (e.g., up to 16% in some regions).

[55] While the estimates made here are sensitive to a number of assumptions, they offer order of magnitude approximations for the contribution of dry N deposition to productivity in coastal upwelling zones; actual values may differ due to variations in particulate aerosol load and N content over interannual cycles. Detailed studies of particulate aerosol load and composition at each of these sites is needed to quantify the role of dry deposition with more accuracy and precision and to determine the role of dry deposition, if any, in supporting productivity and marine food webs in coastal upwelling regions. Our data indicate that the contribution of dry deposition to highly productive coastal upwelling regions is small but not negligible, and could be important during high deposition, nonupwelling periods (e.g., up to 20% of new production in coastal California). Atmospheric nutrient sources are also more important during El Niño periods when upwelling is suppressed, a phenomenon that may become more common due to climate warming. Dry deposition alone may support up to 8% of production in other coastal upwelling regions by providing N and possibly essential Fe and other metals that are required for cell growth but that are deplete in upwelled water.

[56] **Acknowledgments.** We thank M. Jacobson for advice on estimating dry deposition speeds for Monterey Bay; K. Bruland for advice on cellular iron calculations; F. Chavez and R. Michisaki for providing in situ chlorophyll *a* data; E. Gray, C. Buck, and R. Franks for assistance in aerosol extract analysis; and T. L. Kucsera (GEST) at NASA/Goddard for back trajectories (available at aeronet.gsfc.nasa.gov). This research was supported by California Sea grant and NSF grant to A.P. S.M. was a participant in the Stanford Earth Science Intern Program for high school students. K.R.M.M. was supported by the Department of Energy (DOE) Global Change Education Program.

References

Appel, B. R., S. M. Wall, Y. Tokiwa, and M. Haik (1980), Simultaneous nitric acid, particulate nitrate and acidity measurements in ambient air, *Atmos. Environ.*, *14*, 549–554.

Appel, B. R., Y. Tokiwa, and M. Haik (1981), Sampling of nitrates in ambient air, *Atmos. Environ.*, *15*, 549–554.

Bac, M. G., K. R. Buck, F. P. Chavez, and S. C. Brassell (2003), Seasonal variation in alkenones, bulk suspended POM, plankton and temperature in Monterey Bay, California: Implications for carbon cycling and climate assessment, *Org. Geochem.*, *34*, 837–855.

Baker, A. R., M. French, and K. L. Linge (2006), Trends in aerosol nutrient solubility along a west-east transect of the Saharan dust plume, *Geophys. Res. Lett.*, *33*, L07805, doi:10.1029/2005GL024764.

Behrenfeld, M. J., R. T. O'Malley, D. A. Siegel, C. R. McClain, J. L. Sarmiento, G. C. Feldman, A. J. Milligan, P. G. Falkowski, R. M. Letelier, and E. S. Boss (2006), Climate-driven trends in contemporary ocean productivity, *Nature*, *444*, 752–755.

Bonnet, S., and C. Guieu (2004), Dissolution of atmospheric iron in seawater, *Geophys. Res. Lett.*, *31*, L03303, doi:10.1029/2003GL018423.

Boyd, P. W., et al. (2000), A mesoscale phytoplankton bloom in the polar Southern Ocean stimulated by iron fertilization, *Nature*, *407*, 695–702.

Bruland, K. W., J. R. Donat, and D. A. Hutchins (1991), Interactive influences of bioactive trace metals on biological production in oceanic waters, *Limnol. Oceanogr.*, *36*, 1555–1577.

Bruland, K. W., E. L. Rue, and G. J. Smith (2001), Iron and macronutrients in california coastal upwelling regimes: Implications for diatom blooms, *Limnol. Oceanogr.*, *46*, 1661–1674.

Buck, C. S., W. M. Landing, J. A. Resing, and G. T. Lebon (2006), Aerosol iron and aluminum solubility in the northwest Pacific Ocean: Results from the 2002 IOC cruise, *Geochem. Geophys. Geosyst.*, *7*, Q04M07, doi:10.1029/2005GC000977.

Celis, J. E., J. R. Morales, C. A. Zaror, and J. C. Inzunz (2004), A study of the particulate matter PM10 composition in the atmosphere of Chillán, Chile, *Chemosphere*, *54*, 541–550.

Chase, Z., K. S. Johnson, V. A. Elrod, J. N. Plant, S. E. Fitzwater, L. Pickell, and C. M. Sakamoto (2005), Manganese and iron distributions off central California influenced by upwelling and shelf width, *Mar. Chem.*, *95*, 235–254.

Chavez, F. P., and M. Messie (2009), A comparison of eastern boundary upwelling ecosystems, *Limnol. Oceanogr.*, in press.

Chen, Y., and R. L. Siefert (2004), Seasonal and spatial distributions and dry deposition fluxes of atmospheric total and labile iron over the tropical and subtropical North Atlantic Ocean, *J. Geophys. Res.*, *109*, D09305, doi:10.1029/2003JD003958.

Chen, Y., J. Street, and A. Paytan (2006), Comparison between pure-water- and seawater-soluble nutrient concentrations of aerosols from the Gulf of Aqaba, *Mar. Chem.*, *101*, 141–152.

Chen, Y., S. Mills, J. Street, D. Golan, A. Post, M. Jacobson, and A. Paytan (2007), Estimates of atmospheric dry deposition and associated input of nutrients to Gulf of Aqaba seawater, *J. Geophys. Res.*, *112*, D04309, doi:10.1029/2006JD007858.

Chen, Y., A. Paytan, Z. Chase, C. Measures, A. J. Beck, S. A. Sañudo-Wilhelmy, and A. F. Post (2008), Sources and fluxes of atmospheric trace elements to the Gulf of Aqaba, Red Sea, *J. Geophys. Res.*, *113*, D05306, doi:10.1029/2007JD009110.

Chester, R., H. Elderfield, J. J. Griffin, L. R. Johnson, and R. C. Padgham (1972), Eolian dust along the eastern margins of the Atlantic Ocean, *Mar. Geol.*, *13*, 91–105.

Chiapello, I., G. Bergametti, L. Gomes, B. Chatenet, F. Dulac, J. Pimienta, and E. Santos Soares (1995) An additional low layer of Sahelian and Saharan dust over the north-eastern tropical Atlantic, *Geophys. Res. Lett.*, *22*(23), 3191–3194, doi:10.1029/95GL03313.

Chow, J. C., J. G. Watson, E. M. Fujita, Z. Lu, D. R. Lawson, and L. L. Ashbaugh (1994), Temporal and spatial variations of PM sub(2.5) and PM sub(10) aerosol in the Southern California air quality study, *Atmos. Environ.*, *28*, 2061–2080.

Church, T. M., J. M. Tramontano, D. M. Whelpdale, M. O. Andreae, J. N. Galloway, W. C. Keene, A. H. Knap, and J. Tokos Jr. (1991), Atmospheric and precipitation chemistry over the North Atlantic Ocean: Shipboard results, April–May 1984, *J. Geophys. Res.*, *96*, 18,705–18,725.

Coale, K. H., et al. (1996), A massive phytoplankton bloom induced by an eco-system-scale iron fertilization experiment in the equatorial Pacific Ocean, *Nature*, *383*, 495–501.

Codispoti, L. A., R. C. Dugdale, and H. J. Minas (1982), A comparison of the nutrient regimes off northwest Africa, Peru and Baja, California, *Rapp. Proc. Verb. Réun. Int. Counc. Explor Mer.*, *180*, 184–201.

Cornell, S., A. Rendell, and T. Jickells (1995), Atmospheric inputs of dissolved organic nitrogen to the oceans, *Nature*, *376*, 243–246.

Cornell, S. E., T. D. Jickells, J. N. Cape, A. P. Rowland, and R. A. Duce (2003), Organic nitrogen deposition on land and coastal environments: A review of methods and data, *Atmos. Environ.*, *37*, 2173–2191.

Cunningham, E. (1910), On the velocity of steady fall of spherical particles through fluid medium, *Proc. R. Soc., Ser. A*, *83*, 357–365.

Davies, C. N. (1945), Definitive equations for the fluid resistance of spheres, *Proc. Phys. Soc. London*, *57*, 259–270.

Duce, R. A. (1986), The impact of atmospheric nitrogen, phosphorus, and iron species on marine biological productivity, in *The Role of Air-Sea Exchange in Geochemical Cycling*, edited by P. Buat-Menard, pp. 497–529, D. Reidel, Norwell, Mass.

Duce, R. A., and N. W. Tindale (1991), Atmospheric transport of iron and its deposition in the ocean, *Limnol. Oceanogr.*, *36*, 1715–1726.

Duce, R. A., et al. (1991), The atmospheric input of trace species to the world ocean, *Global Biogeochem. Cycles*, *55*(3), 193–259, doi:10.1029/91GB01778.

Duce, R. A., et al. (2008), Impacts of atmospheric anthropogenic nitrogen on the open ocean, *Science*, *320*, 893–897.

Ezat, U., and F. Dulac (1995), Size distribution of mineral aerosols at Amsterdam Island and dry deposition rates in the southern Indian Ocean, *C. R. Acad. Sci., Ser. II*, *320*, 9–14.

Fiebig-Wittmaack, M., E. Schultz, A. M. Córdova, and C. Pizarro (2006), A microscopic and chemical study of airborne coarse particles with particular reference to sea salt in chile at 30°S, *Atmos. Environ.*, *40*, 3467–3478.

Firme, G. F., E. L. Rue, D. A. Weeks, K. W. Bruland, and D. A. Hutchins (2003), Spatial and temporal variability in phytoplankton iron limitation along the California coast and consequences for Si, N, and C biogeochemistry, *Global Biogeochem. Cycles*, *17*(1), 1016, doi:10.1029/2001GB001824.

Friederich, G. E., P. M. Walz, M. G. Burczynski, and F. P. Chavez (2002), Inorganic carbon in the central California upwelling system during the 1997–1999 El Niño–La Niña event, *Prog. Oceanogr.*, *54*, 185–204, doi:10.1016/S0079-6611(02)00049-6.

Geider, R. J., and J. LaRoche (2002), Redfield revisited: Variability of C:N:P in marine microalgae and its biochemical basis, *Eur. J. Phycol.*, *37*, 1–17.

Hansen, H. P., and F. Koroleff (1999), Determination of nutrients, in *Methods of Seawater Analysis*, edited by K. Grasshoff, K. Cremling, and M. Erhardt, pp. 159–228, Wiley, Weinheim, Germany.

Herner, J. D., J. Aw, O. Gao, D. P. Chang, and M. J. Kleeman (2005), Size and composition distribution of airborne particulate matter in northern California: I. Particulate mass, carbon, and water-soluble ions, *J. Air Waste Manage. Assoc.*, *55*, 30–51.

Herut, B., M. D. Krom, G. Pan, and R. Mortimer (1999), Atmospheric input of nitrogen and phosphorus to the southeast Mediterranean: Sources, fluxes, and possible impact, *Limnol. Oceanogr.*, *44*, 1683–1692.

Huebert, B. J. (1980), Nitric acid and aerosol nitrate measurements in the equatorial Pacific region, *Geophys. Res. Lett.*, *7*(5), 325–328, doi:10.1029/GL007i005p00325.

Hutchins, D. A., and K. W. Bruland (1998), Iron-limited diatom growth and Si:N uptake ratios in a coastal upwelling, *Nature*, *393*, 561–564.

Jacobson, M. Z. (2005), Sedimentation, dry deposition, and air-sea exchange, in *Fundamentals of Atmospheric Modeling*, pp. 661–680, Cambridge Univ. Press, New York.

Jaffe, D., S. Tamura, and J. Harris (2005), Seasonal cycle and composition of background fine particles along the west coast of the US, *Atmos. Environ.*, *39*, 297–306.

Jaworski, N. A., R. W. Howarth, and L. J. Hetling (1997), Atmospheric deposition of nitrogen oxides onto the landscape contributes to coastal eutrophication in the northeast United States, *Environ. Sci. Technol.*, *31*, 1995–2004.

Jickells, T. D. (1998), Nutrient biogeochemistry of the coastal zone, *Science*, *281*, 217–222.

Johansen, A. M., R. L. Siefert, and M. R. Hoffmann (2000), Chemical composition of aerosols collected over the tropical North Atlantic Ocean, *J. Geophys. Res.*, *105*(D12), 15,277–15,312, doi:10.1029/2000JD900024.

John, W., R. Kaifer, K. Rahn, and J. J. Wesolowski (1973), Trace element concentrations in aerosols from the San Francisco Bay Area, *Atmos. Environ.*, *7*, 107–118.

Johnson, K. S., F. P. Chavez, V. A. Elrod, S. E. Fitzwater, J. T. Pennington, K. R. Buck, and P. M. Walz (2001), The annual cycle of iron and the biological response in central California coastal waters, *Geophys. Res. Lett.*, *28*(7), 1247–1250, doi:10.1029/2000GL012433.

Kavouras, I. G., P. Koutrakis, F. Cereceda-Balic, and P. Oyola (2001), Source apportionment of PM10 and PM2.5 in five Chilean cities using factor analysis, *J. Air Waste Manage. Assoc.*, *51*, 451–464.

Knap, A., A. Michaels, A. Close, H. Ducklow, and A. Dickson (eds.) (1996), *Protocols for the Joint Global Ocean Flux Study (JGOFS) Core Measurements, JGOFS Rep. 19*, Reprint of the IOC Manuals and Guides 29, UNESCO 1994, pp. 119–122, JGOFS, WHOI, Woods Hole, Mass.

Kouvarakis, G., N. Mihalopoulos, A. Tselepides, and S. Stavrakakis (2001), On the importance of atmospheric inputs of inorganic nitrogen species on the productivity of the eastern Mediterranean Sea, *Global Biogeochem. Cycles*, *15*(4), 805–817, doi:10.1029/2001GB001399.

Krishnamurti, T. N., B. Jha, J. M. Prospero, A. Jayaraman, and V. Ramanathan (1998), Aerosol and pollutant transport and their impact on radiative forcing over tropical Indian Ocean during the January–February, 1996 pre-INDOEX cruise, *Tellus, Ser. B*, *50*, 521–542.

Kudela, R. M., and F. P. Chavez (2000), Modeling the impact of the 1992 El Niño on new production in Monterey Bay, California, *Deep Sea Res., Part II*, *47*, 1055–1076.

Kudela, R. M., and F. P. Chavez (2004), The impact of coastal runoff on ocean color during an El Niño year in Central California, *Deep Sea Res., Part II*, *51*, 1173–1185.

Kudela, R. M., and R. C. Dugdale (2000), Nutrient regulation of phytoplankton productivity in Monterey Bay, California, *Deep Sea Res., Part II*, *47*, 1023–1053.

Lewis, E. R., and S. E. Schwarts (2006), Comment on "Size distribution of sea-salt emissions as a function of relative humidity," *Atmos. Environ.*, *40*, 588–590.

Longhurst, A., S. Sathyendranath, T. Platt, and C. Caverhill (1995), An estimate of global primary production in the ocean from satellite radiometer data, *J. Plankton. Res.*, *17*, 1245–1271.

Mace, K. A., R. A. Duce, and N. W. Tindale (2003), Organic nitrogen in rain and aerosol at Cape Grim, Tasmania, Australia, *J. Geophys. Res.*, *108*(D11), 4338, doi:10.1029/2002JD003051.

Mackey, K. R. M., T. Rivlin, A. R. Grossman, A. F. Post, and A. Paytan (2009), Picophytoplankton responses to changing nutrient and light regimes during a bloom, *Mar. Biol.*, doi:10.1007/s00227-009-1185-2.

Mahowald, N. M., A. R. Baker, G. Bergametti, N. Brooks, R. A. Duce, T. D. Jickells, N. Kubilay, J. M. Prospero, and I. Tegen (2005), The atmospheric global dust cycle and iron inputs to the ocean, *Global Biogeochem. Cycles*, *19*, GB4025, doi:10.1029/2004GB002402.

Martin, J. H., and S. E. Fitzwater (1988), Iron deficiency limits phytoplankton growth in the north-east Pacific subarctic, *Nature*, *331*, 341–343.

Martin, J. H., and G. A. Knauer (1973), The elemental composition of plankton, *Geochim. Cosmochim. Acta*, *37*, 1639–1653.

Mills, M. M., C. Ridame, M. Davey, and J. La Roche (2004), Iron and phosphorus co-limit nitrogen fixation in the eastern tropical North Atlantic, *Nature*, *429*, 292–294.

Moulin, C., C. E. Lambert, F. Dulac, and U. Dayan (1997), Control of atmospheric export of dust from North Africa by the North Atlantic Oscillation, *Nature*, *387*, 691–694.

Nadim, F., M. M. Trahiotis, S. Stapcinskaite, C. Perkins, R. J. Carley, G. E. Hoaga, and X. Yang (2001), Estimation of wet, dry and bulk deposition of atmospheric nitrogen in Connecticut, *J. Environ. Monit.*, *3*, 671–680.

Olivieri, R. A., and F. P. Chavez (2000), A model of plankton dynamics for the coastal upwelling system of Monterey Bay, California, *Deep Sea Res., Part II*, *47*, 1077–1106.

Paerl, H. W. (1985), Enhancement of marine primary production by nitrogen enriched acid rain, *Nature*, *316*, 747–749.

Paerl, H. W., and M. L. Fogel (1994), Isotopic characterization of atmospheric nitrogen inputs as sources of enhanced primary production in coastal Atlantic Ocean waters, *Mar. Biol.*, *119*, 635–645.

Paerl, H. W., J. D. Willey, M. Go, B. L. Peierls, J. L. Pinckney, and M. L. Fogel (1999), Rainfall stimulation of primary production in Western Atlantic Ocean waters: Roles of different nitrogen sources and co-limiting nutrients, *Mar. Ecol. Prog. Ser.*, *176*, 205–214.

Paerl, H. W., R. L. Dennis, and D. R. Whitall (2002), Atmospheric deposition of nitrogen: Implications for nutrient over-enrichment of coastal waters, *Estuaries*, *25*, 677–693.

Parungo, F. P., C. T. Nagamoto, J. Rosinski, and P. L. Haagenson (1986), A study of marine aerosols over the Pacific Ocean, *J. Atmos. Chem.*, *4*, 199–226, doi:10.1007/BF00052001.

Pauly, D., V. Christensen, S. Guénette, T. J. Pitcher, U. R. Sumaila, C. J. Walters, R. Watson, and D. Zeller (2002), Towards sustainability in world fisheries, *Nature*, *418*, 689–695.

Paytan, A., K. R. M. Mackey, Y. Chen, I. D. Lima, S. C. Doney, N. M. Mahowald, R. Labiosa, and A. F. Post (2009), Toxicity of atmospheric aerosols on marine phytoplankton, *Proc. Natl. Acad. Sci. U. S. A.*, *106*, 4601–4605.

Peierls, B. L., and H. W. Paerl (1997), The bioavailability of atmospheric organic nitrogen deposition to coastal phytoplankton, *Limnol. Oceanogr.*, *42*, 1819–1823.

Pennington, J. T., and F. Chavez (2000), Seasonal fluctuations of temperature, salinity, nitrate, chlorophyll, and primary production at station H3/M1 over 1989–1996 in Monterey Bay, CA, *Deep Sea Res., Part II*, *47*, 947–973.

Phinney, L., W. R. Leaitch, U. Lohmann, H. Boudries, D. R. Worsnop, J. T. Jayne, D. Toom-Sauntry, M. Wadleigh, S. Sharma, and N. Shantz (2006), Characterization of the aerosol over the sub-arctic north east Pacific Ocean, *Deep Sea Res., Part II*, *53*, 2410–2433.

Prospero, J. M. (1979), Mineral and sea salt concentrations in various ocean regions, *J. Geophys. Res.*, *84*, 725–731.

Prospero, J. M., and D. L. Savoie (1989), Effect of continental sources on nitrate concentrations over the Pacific Ocean, *Nature*, *339*, 687–689.

Prospero, J. M., K. Barrett, T. Church, F. Dentener, R. A. Duce, J. N. Galloway, H. Levy II, J. Moody, and P. Quinn (1996), Atmospheric deposition of nutrients to the North Atlantic basin, *Biogeochemistry*, *35*, 27–73.

Quinn, P. K., T. S. Bates, J. E. Johnson, D. S. Covert, and R. J. Charlson (1990), Interactions between the sulfur and reduced nitrogen cycles over the central Pacific Ocean, *J. Geophys. Res.*, *95*(D10), 16,405–16,416, doi:10.1029/JD095iD10p16405.

Rhoads, K. P. (1998), The influence of continental emissions on the composition of the remote marine boundary layer, Ph.D. thesis, Univ. of Md., College Park.

Ryan, J., et al. (2008), A coastal ocean extreme bloom incubator, *Geophys. Res. Lett.*, *35*, L12602, doi:10.1029/2008GL034081.

Sadasivan, S. (1978), Trace elements in size separated aerosols over sea, *Atmos. Environ.*, *12*, 1677–1683.

Sarmiento, J. L., et al. (2004), Response of ocean ecosystems to climate warming, *Global Biogeochem. Cycles*, *18*, GB3003, doi:10.1029/2003GB002134.

Savoie, D. L., and J. M. Prospero (1977), Aerosol concentration statistics for the northern tropical Atlantic, *J. Geophys. Res.*, *82*, 5945–5964, doi:10.1029/JC082i037p05954.

Savoie, D. L., and J. M. Prospero (1982), Particle-size distribution of nitrate and sulfate in the marine atmosphere, *Geophys. Res. Lett.*, *9*(10), 1207–1210, doi:10.1029/GL009i010p01207.

Savoie, D. L., J. M. Prospero, and R. T. Nees (1987), Nitrate, non-sea-salt sulfate, and mineral aerosol over the northwestern Indian Ocean, *J. Geophys. Res.*, *92*(D1), 933–942, doi:10.1029/JD092iD01p00933.

Schaap, M., et al. (2004), Artifacts in the sampling of nitrate studied in the "INTERCOMP" campaigns of EUROTRAC-AEROSOL, *Atmos. Environ.*, *38*, 6487–6496.

Seitzinger, S. P., and R. W. Sanders (1999), Atmospheric inputs of dissolved organic nitrogen stimulate estuarine bacteria and phytoplankton, *Limnol. Oceanogr.*, *44*, 721–730.

Slinn, S. A., and W. G. N. Slinn (1980), Predictions for particle deposition on natural waters, *Atmos. Environ.*, *14*, 1013–1016.

Spokes, L. J., and T. D. Jickells (1996), Factors controlling the solubility of aerosol trace metals in the atmosphere and on mixing into seawater, *Aquat. Geochem.*, *1*(4), 355–374, doi:10.1007/BF00702739.

Spokes, L. J., T. D. Jickells, and K. Jarvis (2001), Atmospheric inputs of trace metals to the northeast Atlantic Ocean: The importance of southeasterly flow, *Mar. Chem.*, *76*, 319–330.

Sunda, W. G., and S. A. Huntsman (1995), Iron uptake and growth limitation in oceanic and coastal phytoplankton, *Mar. Chem.*, *50*, 189–206.

Takeda, S. (1998), Influence of iron availability on nutrient consumption ratio of diatoms in oceanic waters, *Nature*, *393*, 774–777.

Uematsu, M., R. A. Duce, J. M. Prospero, L. Chen, J. T. Merrill, and J. T. Mc Donald (1983), Transport of mineral aerosol from Asia over the Pacific Ocean, *J. Geophys. Res.*, *88*(C9), 5345–5352, doi:10.1029/JC088iC09p05343.

Valigura, R. A., W. T. Luke, R. S. Artz, and B. B. Hicks (1996), Atmospheric nutrient input to coastal areas: Reducing the uncertainties, *Decision Anal. Ser. 9*, NOAA Coastal Ocean Program, Silver Spring, Md.

VanCuren, R. A. (2003), Asian aerosols in North America: Extracting the chemical composition and mass concentration of the Asian continental aerosol plume from long-term aerosol records in the western United States, *J. Geophys. Res.*, *108*(D20), 4623, doi:10.1029/2003JD003459.

Volpe, G., V. F. Banzon, R. H. Evans, R. Santoleri, A. J. Mariano, and R. Sciarra (2009), Satellite observations of the impact of dust in a low-nutrient, low-chlorophyll region: Fertilization or artifact?, *Global Biogeochem. Cycles*, *23*, GB3007, doi:10.1029/2008GB003216.

Wagener, T., C. Guieu, R. Losno, S. Bonnet, and N. Mahowald (2008), Revisiting atmospheric dust export to the Southern Hemisphere ocean: Biogeochemical implications, *Global Biogeochem. Cycles*, *22*, GB2006, doi:10.1029/2007GB002984.

Wang, H. C., and W. John (1988), Characteristic of the Berner Impactor for sampling inorganic ions, *Aerosol Sci. Technol.*, *8*, 157–172.

Wara, M. W., A. C. Ravelo, and M. L. DeLaney (2005), Permanent El Niño-like conditions during the Pliocene warm period, *Science*, *309*, 758–761.

Wells, K. C., M. Witek, P. Flatau, S. M. Kreidenweis, and D. Westphal (2007), An analysis of seasonal surface dust aerosol concentrations in the western U.S. (2001–2004): Observations and model predictions, *Atmos. Environ.*, *41*, 6585–6597.

Wilkerson, F. P., R. C. Dugdale, A. Marchi, and C. A. Collins (2002), Hydrography, nutrients, and chlorophyll during El Niño and La Niña 1997–99 winters in the Gulf of the Farrallones, California, *Prog. Oceanogr.*, *54*, 293–310.

Williams, R. M. (1982), A model for the dry deposition of particles to natural water surfaces, *Atmos. Environ.*, *16*, 1933–1938.

Wollast, R. (1991), The coastal organic carbon cycle: Fluxes, sources and sinks, in *Ocean Margin Processes in Global Change*, edited by R. C. F. Mantoura et al., pp. 365–382, Wiley, Chichester, U. K.

Zorn, S. R., F. Drewnick, M. Schott, T. Hoffmann, and S. Borrmann (2008), Characterization of the South Atlantic marine boundary layer aerosol using an aerodyne aerosol mass spectrometer, *Atmos. Chem. Phys.*, *8*, 4711–4728.

K. R. Arrigo and G. L. van Dijken, Department of Environmental Earth System Science, Stanford University, Stanford, CA 94305, USA.

A. M. Erhardt and S. Mazloom, Department of Geological and Environmental Sciences, Stanford University, Stanford, CA 94305, USA.

K. R. M. Mackey, Department of Civil and Environmental Engineering, Stanford University, Stanford, CA 94305, USA. (kmackey@stanford.edu)

A. Paytan, Institute of Marine Science, University of California, A317 Earth and Marine Sciences Bldg., 1156 High St., Santa Cruz, CA 95064, USA.

J. Ryan, Monterey Bay Aquarium Research Institute, 7700 Sandholdt Rd., Moss Landing, CA 95039-9644, USA.